Quantitative Global Assessment of Land Degradation and Improvement:
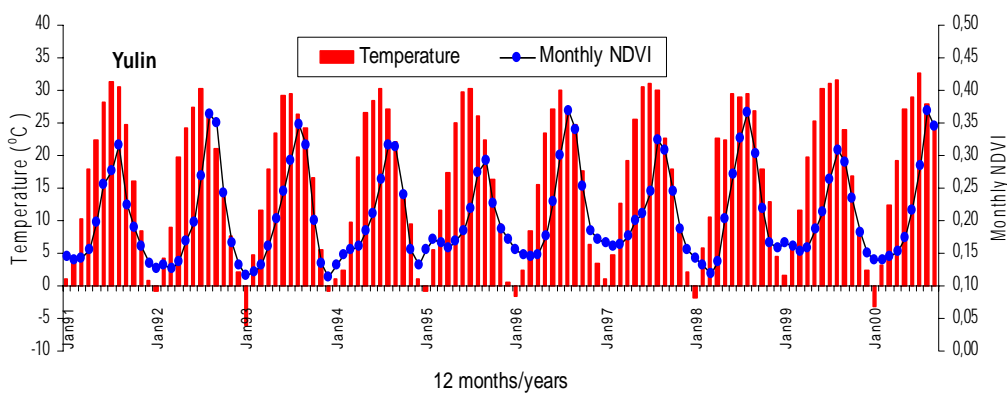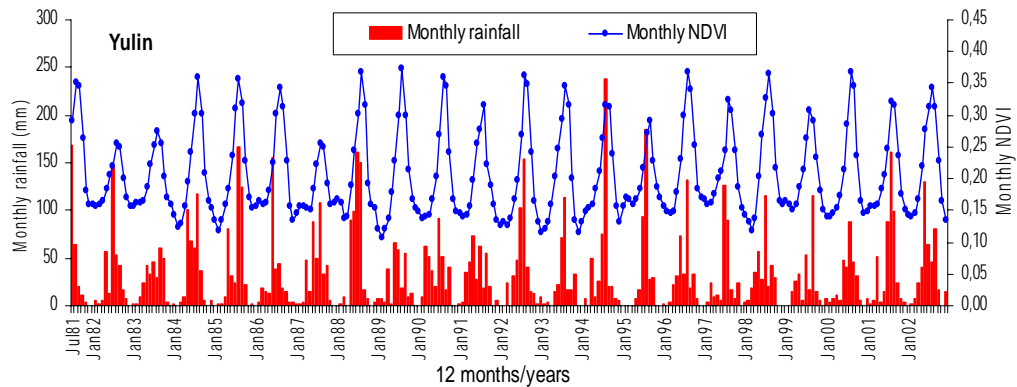# pilot study in North China

Z G Bai
D L Dent
M E Schaepman

(May 2005)

ISRIC World Soil Information

WAGENINGEN UNIVERSITY
WAGENINGEN UR

Disclaimer:
While every effort has been made to ensure that the data are accurate and reliable, ISRIC cannot assume liability for damages caused by inaccuracies in the data or as a result of the failure of the data to function on a particular system. ISRIC provides no warranty, expressed or implied, nor does an authorized distribution of the data set constitute such a warranty. ISRIC reserves the right to modify any information in this document and related data sets without notice.

Correct citation:
Bai ZG, Dent DL, Schaepman ME 2005 Quantitative Global Assessment of Land Degradation and Improvement: pilot study in North China. Report 2005/06, ISRIC – World Soil Information, Wageningen.

Inquiries:
c/o Director, ISRIC – World Soil Information
PO Box 353
6700 AJ Wageningen
The Netherlands
Telefax: +31-(0)317-471700
E-mail: soil.isric@wur.nl
Web: www.isric.org

Contents

LIST OF FIGURES

LIST OF TABLES

EXECUTIVE SUMMARY

Land degradation is believed to be a severe and widespread environmental problem. It is pivotal to the United Nations Convention to Combat Desertification, the Convention on Biodiversity, and the Kyoto Protocol on Global Climatic Change. However, there is no authoritative measure of land degradation and countervailing land improvements; there is pressing need for an up-to-date, quantitative and reproducible assessment to support policy development for food and water security, environmental integrity, international aid programs, and national strategies for economic development and resource conservation.

A quantitative global assessment of land degradation and improvement (GLADA) is proposed to identify: 1) the status and trends of land degradation; 2) *hotspots* suffering extreme constraints or at severe risk and their counterpoints - areas where degradation has been arrested or reversed. The objective of this pilot in North China is to develop a methodology using the 22-year NOAA-AVHRR GIMMS dataset of NDVI data and ancillary information to: i) test procedures for handling the dataset and build a NDVI database and ii) develop algorithms for analysis of the data.

Two approaches have been followed:

Statistical Indicators: The GIMMS NDVI data were extracted and geo-referenced. Algorithms were developed to calculate indicators of land degradation: NDVI minimum, maximum, maximum-minimum, mean, sum, and coefficient of variation (CoV). Annual, growing season (May-October) and non-growing season (November-April) indicators were derived for each pixel; their temporal trends were determined by linear regression at annual intervals and mapped to depict spatial changes. A negative regression coefficient over several years indicates a decline of green biomass (by inference, land degradation if not accounted for by land use change) and a positive regression coefficient, an increase (land improvement).

Modelling: An NDVI database for Eurasia was developed in MS Access. Spatial patterns of NDVI were compared with and combined with rainfall, temperature, net primary productivity (NPP) and land degradation information derived from the study area. Structured query language (SQL) was applied to query and calculate NDVI indicators and biophysical parameters. Subsequently, correlations of the NDVI indicators and their relationships with rainfall, temperature, net primary productivity (NPP) and rainfall-use efficiency (RUE) were statistically analyzed. ArisFlow was used to analyse the NDVI datasets; the HANTS algorithm was used to smooth and reconstruct the NDVI time-series and remove extreme values that might affect generalizations.

Correlations between the NDVI indicators are low to moderate (r^2 0.25 – 0.66) except for a very high correlation between mean and sum of NDVI (r^2 = 1), which may be considered alternates. Similar relations for their temporal trends, identified by the slopes of linear regressions, were found for the study area. Relations of the NDVI indicators and net primary productivity (NPP) with annual rainfall are only moderate, but high with monthly rainfall. The correlations between rain-use efficiency, calculated as the ratio between NPP and rainfall (RUE_{NPP}) and as ratio NDVI:rainfall (RUE_{NDVI}), are statistically significant ($P < 0.001$), and higher for the monthly intervals; they can be considered alternates.

The results indicate that all NDVI indicators have biological meaning. Overall, green biomass increased over the 22-year period without close correspondence with annual rainfall; rather, there is a lag of a few years between diminished rainfall and diminished biomass production. Signs of declining green biomass production, indicating active land degradation, are localised. Where a diminishing trend is evident, this is clearly shown in the shape of the annual NDVI curve, which is attenuated well before climax of the growing season. Rain-use efficiency increased at Yulin, indicating land improvement, and decreased at Dingbian.

This study has not considered whether the increase in green biomass, expressed as NDVI, has improved land quality. However, increased vegetation cover will decrease soil erosion and increase infiltration, water storage and soil organic matter. When this is demonstrated by field validation, the indices developed here could be used as input for an early warning system for land degradation.

Keywords: Land degradation, remote sensing, North China, early warning system, NOAA-AVHRR, GIMMS NDVI

1. INTRODUCTION AND OBJECTIVES

Land degradation is believed to be a severe and widespread environmental problem (Dregne *et al.* 1991, Reynolds & Stafford Smith 2002, UNCED 1992). It is pivotal to the United Nations Convention to Combat Desertification, the Convention on Biodiversity, and the Kyoto Protocol on Global Climatic Change. However, there is no authoritative measure of land degradation and countervailing land improvements. The only harmonized global assessment of land degradation is the Global Assessment of Human-Induced Soil Degradation (GLASOD) (Oldeman *et al.* 1991). It is a map of perceptions - the kinds, degree and relative extent of degradation, not a measure of degradation; and now out-of-date - land degradation and perceptions have moved on. There is pressing need for an up-to-date, quantitative and reproducible assessment of land degradation and improvement to support policy development for food and water security, environmental integrity, international aid programs, and national strategies for economic development and resource conservation. A quantitative global assessment of land degradation and improvement (GLADA) is now proposed to identify the status and trends of land degradation, *hotspots* suffering severe degradation or at severe risk, and their counterpoint - areas where degradation has been arrested or reversed.

Biomass is an integrated measure of biological productivity. Its deviance from the norm may be taken as a measure of land degradation or improvement. Global satellite data, in particular the normalized difference vegetation index (NDVI)[1] or greenness index, enable measurement of changes in biomass from the field and local validation scale (1:10 000) to the degree of generalization required for national and regional action, or to support international policy development (1:1 million to 1:5 million). Local and regional norms may be calculated by stratifying the land area according to climate, soils and terrain, and land use/vegetation; deviance may then be calculated locally and regionally.

NDVI has a strong linear relationship with the fraction of photosynthetically active radiation absorbed by the plant (Asrar *et al.* 1984, Sellers 1987, Sellers *et al.* 1997); many studies have shown strong correlation between NDVI and vegetation cover (e.g. Purevdoj *et al.* 1998) and above-ground net primary productivity (Running and Nemani 1988, Potter *et al.* 1993, Paruelo *et al.* 1997, Wang *et al.* 2004); so NDVI has been applied in the studies of land degradation at local and regional scales (e.g. Asner *et al.* 2003, 2004, Archer 2004, Asner and Heidebrecht 2005, Bastin *et al.* 1995,

---

[1] NDVI is the difference in reflectance between the AVHRR near-infrared and visible bands, divided by the sum of these two bands (Sellers 1985, Sellers *et al.* 1994, Tucker 1980).

Bradley and Mustard 2005, Budde *et al*. 2004, Diouf and Lambin 2001, Evans and Geerken 2004, Geerken and Ilaiwi 2004, Holm *et al.* 2003, Li *et al*. 2004, Maselli *et al.* 1998, 2003, Millch and Weiss 2000, Mouat *et al*. 1997, Nicholson *et al*. 1998, Pelkey *et al*. 2000, Prince *et al*. 1998, Ringrose *et al*. 1996, Runnström 2000 2003a b, Singh *et al*. 2004 2005, Stoms and Hargrove 2000, Symeonakis and Drake 2004, Tanser and Palmer 1999, Thiam 2003, Tottrup and Rasmussen 2004, Tucker *et al*. 1991a b, Weiss *et al.* 2001 2004).

The objective of this pilot is to develop a methodology for assessing land degradation and improvement using NOAA-AVHRR time-series data and ancillary information - specifically to: i) test procedures for handling of the dataset and building an NDVI database, ii) develop algorithms for analysis of the data, iii) analyze the NDVI deviations and trends in the study area.
The following sections deal with: (2) an overview of the study area and the datasets used for the study; (3) the methodology developed so far – data handling procedures, statistical analysis of NDVI indicators of degradation and improvement, data modelling and GIS analysis; (4) results, a brief discussion of the results in relation to the study area, and assessment of the potential usefulness of the different NDVI and derived indicators of land degradation and improvement; (5) summary and conclusions.

2.   STUDY AREA AND DATASETS

2.1   Study area

The pilot area is Yulin Prefecture, Shaanxi Province, North China, latitude 36˚ 57′ – 39˚ 34′ N and longitude 107˚ 28′ - 111˚ 15′ E. It encompasses twelve counties: Yulin (Yuyang district), Shenmu, Fugu, Jiaxian, Mizhi, Suide, Wubu, Zizhou, Qinjian, Hengshan, Jingbian and Dingbian which encompass 42 986 km^2 with some 3.4 million inhabitants (Figs. 1a; 1b). It is a transitional zone between the Mu Us Desert and the Loess Plateau; sandy land, in the northern part, and hilly loess, in the middle-south, each make up about half of the area. Elevation increases from the southeast to the northwest; mean elevation is 1000m above sea level, the maximum is 1907m on Mount Baiyun. Climate ranges from arid in the northwest to sub-humid in the southeast: spring is dry and windy, summer short and hot with rainfall maximum, autumn brings short rains, followed by a long dry and cold winter. Mean maximum temperature is 32°C, mean minimum -6.1°C. At Yulin, mean annual rainfall is 396mm, ranging from 159-695mm (1934 to 2003); at Dingbian, mean annual rainfall is 293mm, ranging from 145 to 587mm (1954 to 1996). Most of the rain falls in July and August, and there

is a large inter-annual variation; spatially, rainfall decreases from the southeast towards the northwest. Soils are Kastanozems and Arenosols (WRB 2005) with natural vegetation grading from forest steppe, through steppe, to desert.

It is an agro-pastoral region with important coal and oil exploitation – a diverse but vulnerable environment in which rampant land degradation has been reported by several observers (Liu 1996, Wu 1996, Gao *et al*. 2001, Zhang *et al*. 2002, Liu and Gao 2002, Liu *et al*. 2003 (see Appendix I), Runnström 2000 2003a b, Li *et al.* 2004). Land degradation is reported to be a severe environmental problem with social and economic implications (Li 1998).
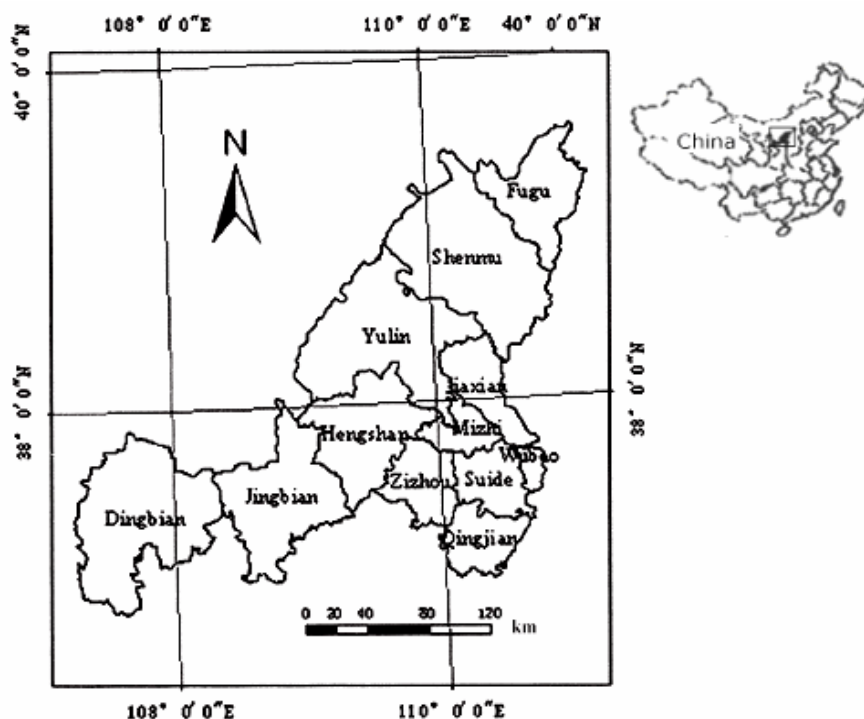
Figure 1a. Location of GLADA pilot in North China
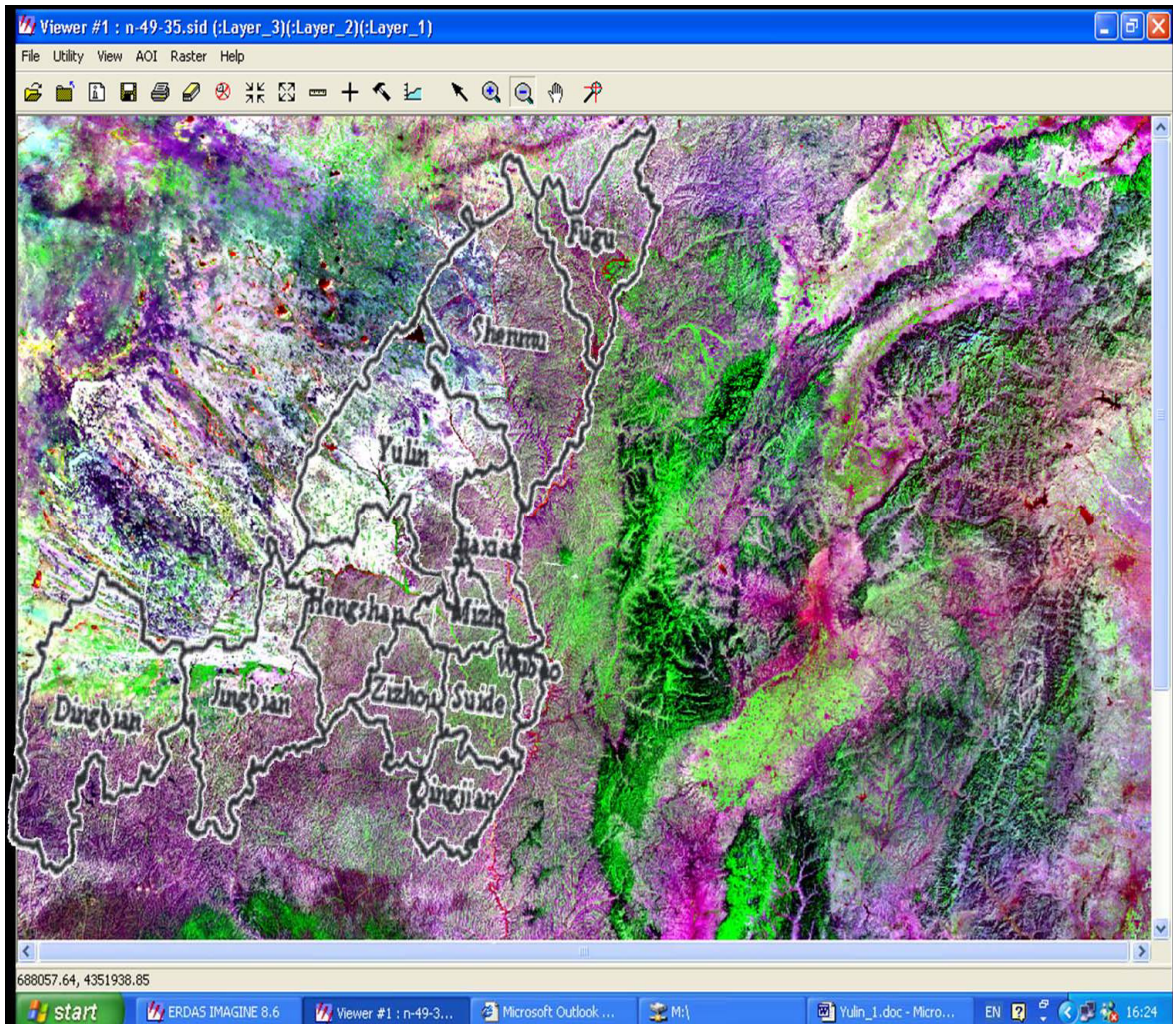
Figure 1b.   Image of the study area from Landsat4/5 1990
                  (*source: zulu.ssc.nasa.gov.mrsid)*

2.2 Datasets

2.2.1 GIMMS datasets

The Global Inventory Modelling and Mapping Studies (GIMMS) dataset was collected between 1981 and 2002 by the advanced very high resolution radiometer (AVHRR) on National Oceanic and Atmospheric Administration (NOAA) satellites. It comprises two-weekly NDVI images with 8km spatial resolution, corrected for calibration, view geometry, volcanic aerosols, and other effects unrelated to vegetation change (Tucker *et al.* 2004). The accuracy of GIMMS is proven to be suitable for a global assessment; precursors were used to derive greenness trends in the Northern

Hemisphere (Myneni *et al.* 1997) and assess vegetation cover and erosion classes (Hochschild *et al.* 2003).

2.2.2 Climatic and biomass data

Daily rainfall and temperature data are available for Yulin and Dingbian. Monthly net primary productivity (NPP) data (1981-1998) derived from the Carbon Exchange between Vegetation, Soil and Atmosphere (CEVSA) model (Cao and Woodward 1998a b) were provided by Tao *et al.* (personal communication). Data for land degradation status for six counties (Dingbian, Jingbian, Hengshan, Yulin, Shenmu, and Fugu) were provided by Liu *et al.* (2003).

3. METHODOLOGY

Two approaches have been developed to assess land degradation: statistical analysis and spatial modelling. Figures 2 and 3 depict the sequence of activities.

3.1 Statistical analysis of NDVI indicators

NDVI data were extracted and geo-referenced using ERDAS IMAGINE and ArcGIS. Algorithms were developed to calculate indicators of land degradation, namely: NDVI minimum, maximum, maximum-minimum, mean, sum, and coefficient of variation (CoV). Annual, growing season (May-October) and non-growing season (November-April) indicators were derived for each pixel; their temporal trends were determined by linear regression at annual intervals. A negative regression coefficient indicates a decline of green biomass and a positive regression coefficient, an increase - except for CoV which indicates trends in variability.

```
┌──────────────────┐                    ┌──────────────────┐
│  GIMMS dataset   │                    │ Map of the study │
│                  │                    │       area       │
└──────────────────┘                    └──────────────────┘
         │                                       │
         ▼                                       ▼
      ╱────────╲                             ╱────────╲
     ╱  ERDAS   ╲                           ╱  ArcGIS  ╲
    ╱   Geo-     ╲                         ╱    Re-     ╲
    ╲ referencing╱                         ╲ projecting ╱
     ╲          ╱                           ╲          ╱
      ╲────────╱                             ╲────────╱
         │                                       │
         ▼                                       ▼
┌──────────────────┐                    ┌──────────────────┐
│  Geo-referenced  │                    │ Re-projected map │
│   NDVI images    │                    │                  │
└──────────────────┘                    └──────────────────┘
         │              ╱────────╲               │
         └────────────▶╱  Clip to ╲◀─────────────┘
                       ╲ the study╱
                        ╲  area   ╱
                         ╲───────╱
                             │
                             ▼
                  ┌──────────────────────┐
                  │  NDVI images of the  │
                  │      study area      │
                  └──────────────────────┘
                             │
                             ▼
                       ╱──────────╲
            ┌─────────╱ Algorithm   ╲─────────┐
            │         ╲ development & ╱        │
            │          ╲calculations╱         │
            ▼           ╲ of NDVI  ╱          ▼
       ╱────────╲        ╲deviation╱     ╱────────╲
      ╱  ERDAS   ╲        ╲───────╱     ╱  ArcGIS  ╲
      ╲ process  ╱                      ╲ display  ╱
       ╲────────╱                        ╲────────╱
            │                                 │
            └──────────────┐   ┌──────────────┘
                           ▼   ▼
            ┌──────────────────────────────────┐
            │ Spatio-temporal patterns of NDVI │
            │            parameters            │
            └──────────────────────────────────┘
```
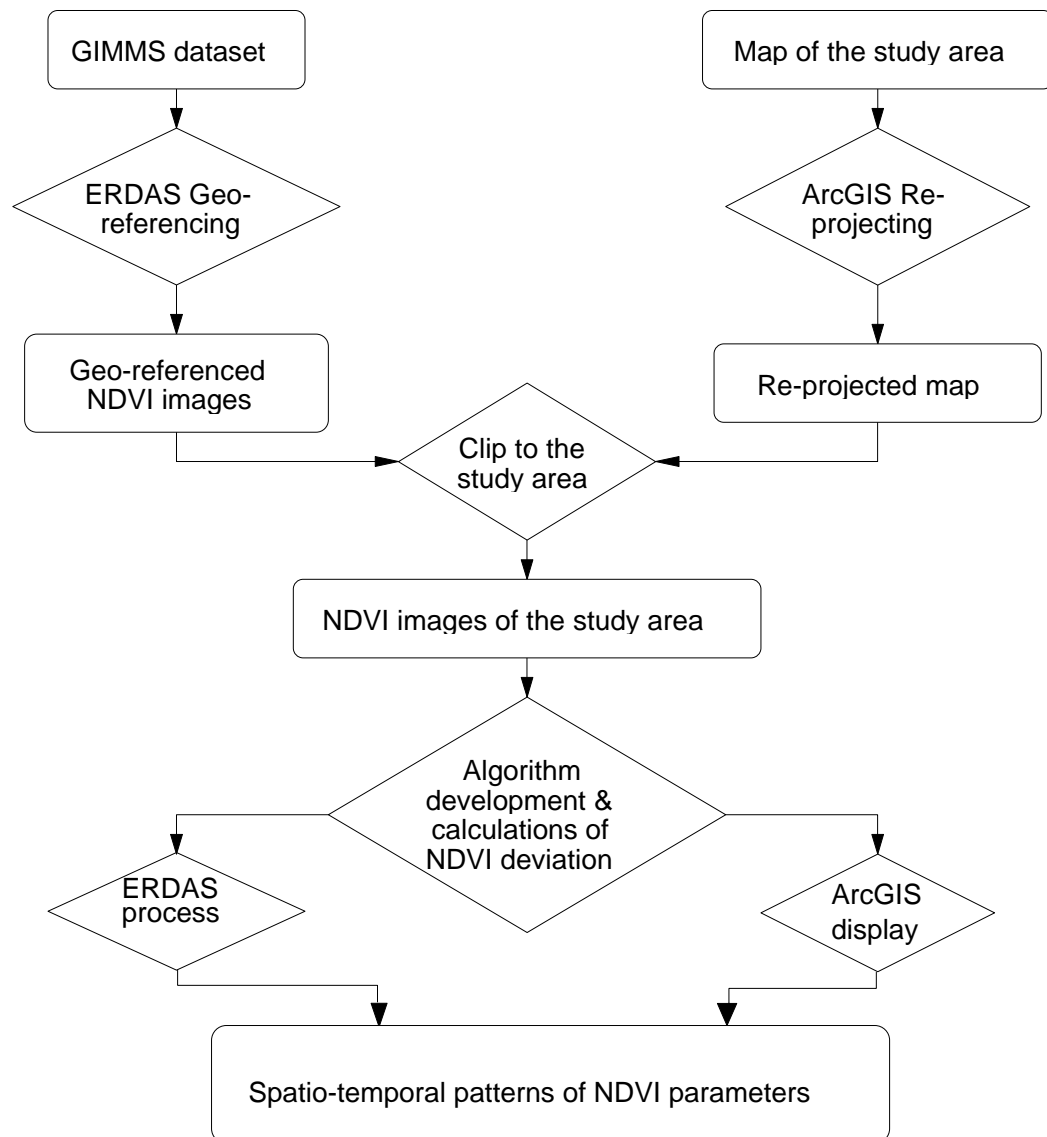
Figure 2.   Flowchart of the procedures for statistical analysis

3.2 Modelling

In the modelling approach, the GIMMS NDVI images of the Eurasian continent (1981-2002) and their longitude and latitude images were extracted and converted into *.dat and *.txt formats using ERDAS IMAGINE 8.6 and UltraEdit software, respectively, and imported into MS Access. The database was automatically geo-referenced for each pixel with unique identifier (ID) from 1 to 2.5 million.

The topographic map of the six counties discussed in Appendix 1 was digitized and geometrically transformed to the same projection as the GIMMS data set (Albers conical equal-area projection with the Clark ellipsoid) using ground control points. The identifiers of the NDVI pixels within each sub-area (Chinas_ID) were identified and imported into MS Access.

The land degradation indicators and geo-located climate and biomass data were imported into MS Access to create four datasets:

NDVI81_02: 22-year NDVI values. For example, **Ea8108a** means Eurasia NDVI values in year 1981 and the first half of the August (08a), other attributes of the entity NDVI81_02 can be read as the same way except the change in years and months.

Sub-area and severity level: The independent assessment of land degradation from Liu *et al.* 2003; consists of sub-area_ID and the land degradation severity of the six counties. Sub-area_ID is defined as a primary key.

LD_criteria: The land degradation indicators derived from Liu *et al.* 2003. The *-min* and *-max* values are the criteria used to indicate the minimum and maximum range of the indicators. For example, severe land degradation (level I) is defined as vegetation coverage <10 per cent.

Climate and biomass: Monthly net primary productivity data from 1981 to 1998 and monthly rainfall data between 1981 and 2002 for Yulin and Dingbian, and their locations.

Data modelling (Watson 1999), structured query language (SQL) and statistics were used to generate indicators for vegetation, land degradation or improvement and further analyses (Figs. 3 and 4).
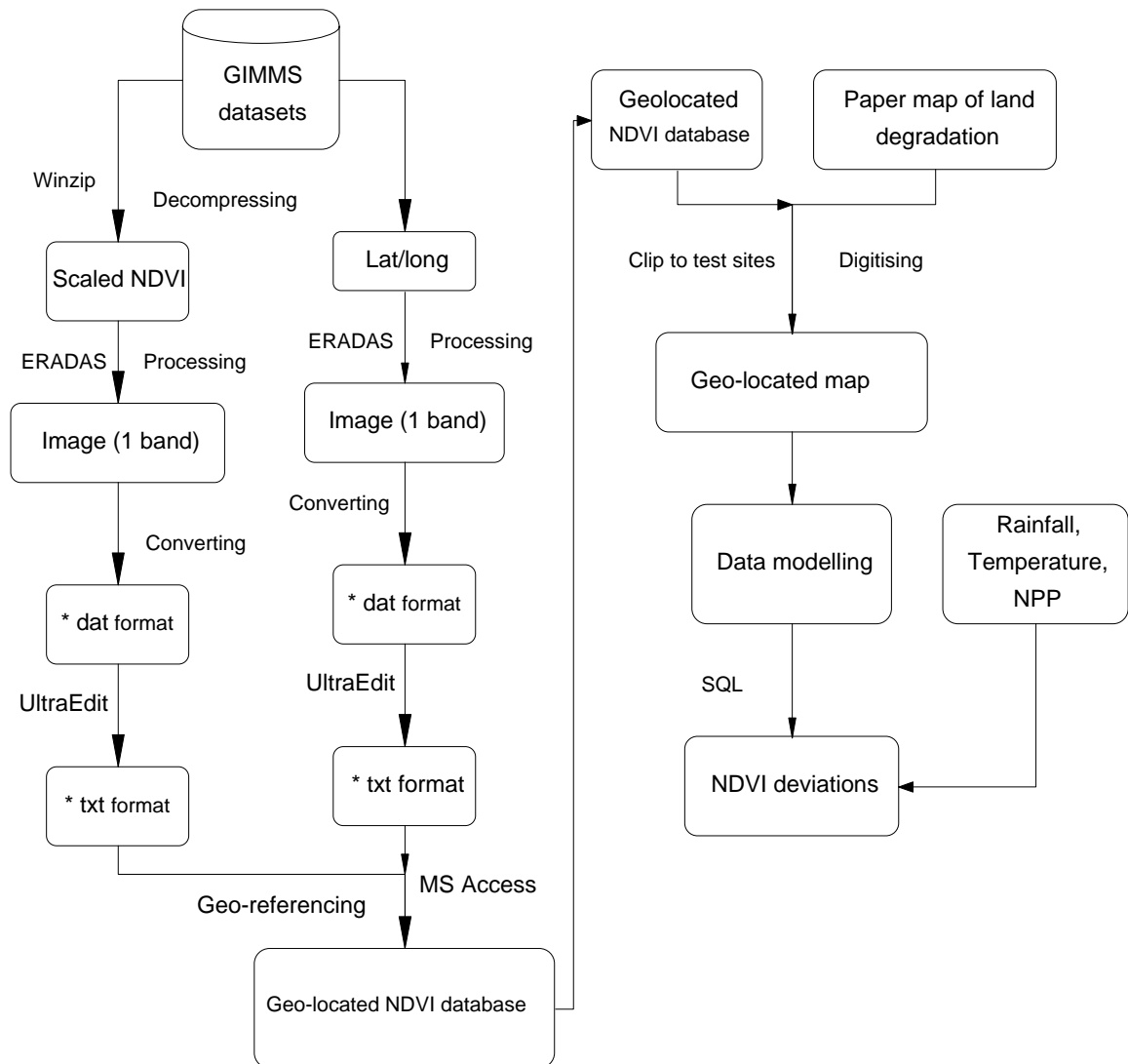
Figure 3.   Procedures for modelling
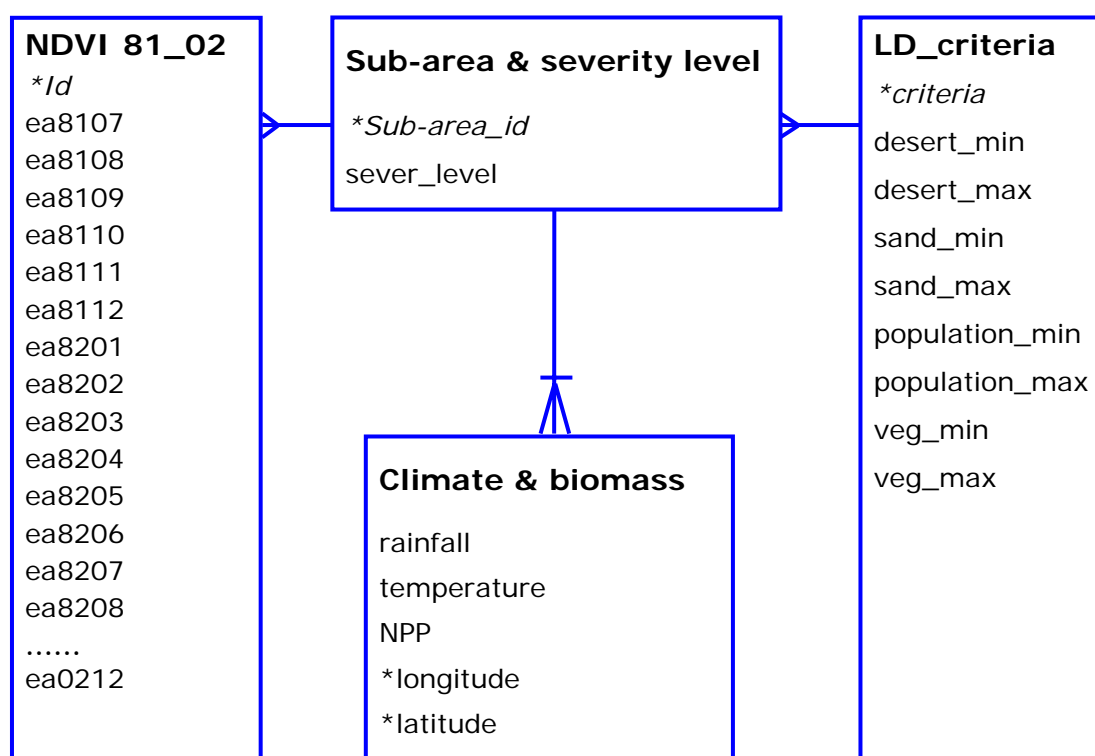
Figure 4.   Data modelling diagram

4.   RESULTS AND DISCUSSION

4.1   Trends in NDVI indicators

Table 1 summarises the values of the NDVI indicators for annual, growing season and non-growing season periods. Temporal trends for each pixel, determined by the slope of the linear regression equation, were classed as *no change* (slope <0.0001 and >-0.0001), *increase* (positive slope ≥0.0001), and *decrease* (negative slope ≤-0.0001). Spatial patterns are depicted in Figures 5 to 10.

Minimum NDVI

The minimum NDVI is the lowest value that occurs in any one year (annual) which is almost invariably at the end of winter, any one growing season, or any one non-growing season. Fig. 5 shows the spatial patterns and temporal trends of multi-year mean annual-, growing season-, and non-growing season minimum NDVI. Over the 22-year period: annual values tended to increase over 67% of pixels, 23% decreased and 10% remained

unchanged; for the non-growing season, the picture is much the same with increase in 73% of pixels, decrease in 17% and 10% unchanged; but for the growing season, 90% increased, 6% were unchanged and only 4% decreased.

The different behaviour of the three indicators might be attributed to land use change (Li *et al.* 2004, Fig. 12): conversion of barren land to grassland would increase minimum biomass in the growing season; in contrast, change from grassland to arable would decrease minimum green biomass (NDVI) in the non-growing period.

Correlation between annual rainfall and minimum NDVI is relatively low (Table 6) so variation in minimum NDVI should be used with caution as an indictor of land degradation or recovery. However, it serves as a baseline for other parameters.

Table 1.   Statistics of NDVI indicators

NDVI indicators	Range (minimum, maximum, mean)			No change no. (%)	Increase no. (%)	Decrease no. (%)
annually						
Minimum NDVI	0.006	0.105	0.08	80 (10)	537 (67)	182 (23)
Maximum NDVI	0.006	0.663	0.445	1 (0.1)	798 (99.9)	0
Max-min NDVI	0.000273	0.324	0.189	25 (3)	769 (96)	5 (1)
Mean NDVI	0.006	0.263	0.192	41 (5)	726 (91)	32 (4)
Sum NDVI	3.1	138	100.6	1 (0.1)	778 (96.9)	20 (3)
NDVI CoV	0.00074	0.472	0.307	24 (3)	738 (92)	37 (5)
Growing season						
Minimum NDVI	0.006	0.15	0.115	45 (6)	720 (90)	34 (4)
Maximum NDVI	0.006	0.663	0.445	57 (7)	738 (92)	4 (1)
Max-min NDVI	0.003	0.591	0.375	35 (4)	720 (90)	44 (6)
Mean NDVI	0.006	0.338	0.241	41 (5)	746 (93)	12 (2)
Sum NDVI	1.6	89	63.5	1 (0.1)	746 (92.9)	52 (7)
NDVI CoV	0.00037	0.316	0.196	44 (6)	454 (57)	301 (38)
Non-growing season						
Minimum NDVI	0.006	0.176	0.119	77 (10)	579 (73)	143 (17)
Maximum NDVI	0.006	0.247	0.17	48 (6)	714 (89)	37 (5)
Max-min NDVI	0.003	0.108	0.049	0	799 (100)	0
Mean NDVI	0.006	0.201	0.142	70 (9)	636 (80)	93 (11)
Sum NDVI	1.6	53.1	37.2	24 (3)	661 (83)	114 (14)
NDVI CoV	0.001	0.181	0.102	42 (5)	681 (85)	76 (10)

Maximum NDVI

Maximum NDVI represents the maximum green biomass. The patterns of monthly maximum NDVI (Fig. 14), personal experience and communication with local experts suggest that peak biomass occurs between late July and early September, mostly in August.

The large spatial variation in maximum NDVI reflect the diverse landscape and climate but the 22-year trends of annual and growing-season values are positive almost everywhere in the study area (Fig. 6). Over the 22-year period, annual and growing-season maximum NDVI increased over 93% of the area while 7% remained unchanged. For the non-growing period, it tended to increase over 89% of the area, remained unchanged over 6%, while 5% decreased.

Maximum-minimum NDVI

The difference between maximum and minimum NDVI over the year reflects biomass production. For both annual and growing season max-min NDVI, more than 90% of the pixels tended to increase, 3-4% remained unchanged, while less than 5% decreased (Fig. 7).

Mean NDVI

Fig. 8 shows the spatial pattern of multiyear average mean NDVI and their trends. The spatial patterns of growing season mean NDVI and annual mean are the same, so are the slope coefficients of their linear regression equations: more than 91% of the pixels increased, 5% remained unchanged and less than 4% decreased. For non-growing season, however, more than 11% of the total pixels were negative, 9% remained unchanged and 80% positive.

Correlations between annual rainfall and mean NDVI were weak at Yulin and moderate at Dingbian (Table 6). Inter-annual variability in rainfall would not be reflected in the variance of both trends and magnitude of the mean NDVI.

Sum or integrated NDVI

The sum of fortnightly NDVI values for the year (annual) and for the growing season, most nearly integrates biomass and biomass production, respectively.

The spatial distribution of the annual and growing season sum NDVI are similar; likewise, the slope coefficients of their linear regression equations (Fig. 9). Rather more pixels with negative slopes occurred for the growing season (52) than for the annual sum NDVI (12 pixels).

The pattern of integrated NDVI was very similar to the max-min and mean NDVI: for the annually integrated NDVI 97% of the total pixels increased; 93% increased for the growing season.

Figure 5.   Mean minimum NDVI 1981-2002: top left - annual; middle left - growing season (May-Oct);
bottom left – non-growing season (Nov-Apr). Classified maps of slope coefficients of linear regression for
minimum NDVI: top right - annual; middle right - growing season; bottom right - non-growing season

Mean annual maximum NDVI

Slope of annual maximum NDVI

Mean growing season maximum NDVI

Slope of growing season maximum NDVI

Mean non-growing season maximum NDVI

Slope of non-growing maximum NDVI

Figure 6.   Mean maximum NDVI 1981-2002: top left - annual; middle left - growing season (May-Oct); bottom left - non-growing season (Nov-Apr). Classified maps of slope coefficients of linear regression for maximum NDVI: top right - annual; middle right - growing season; bottom right - non-growing season
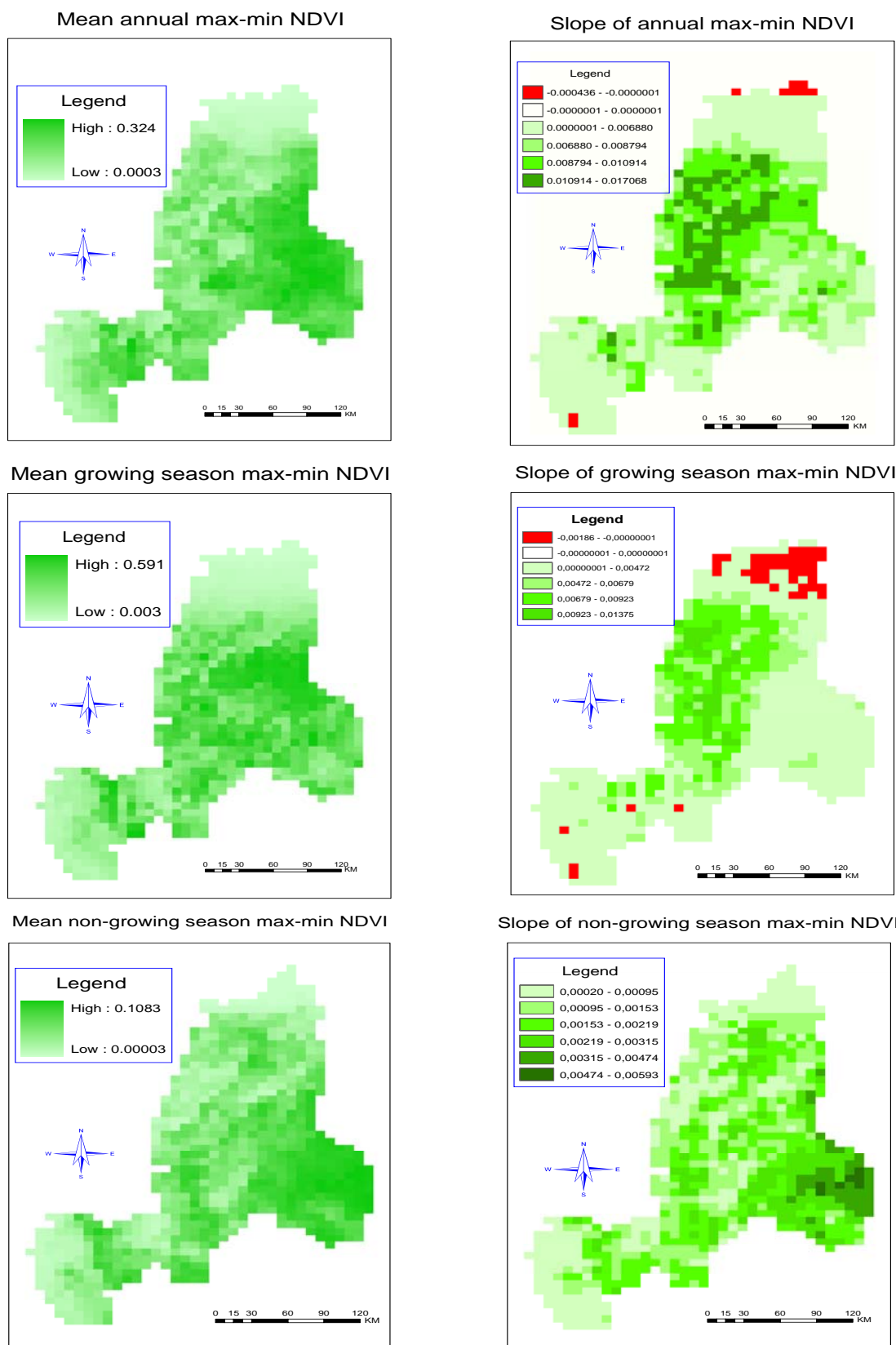
Figure 7. Mean maximum-minimum NDVI 1981-2002: top left - annual; middle left - growing season (May-Oct); bottom left - non-growing season (Nov-Apr). Classified maps of slope coefficients of linear regression for maximum-minimum NDVI: top right - annual; middle right - growing season; bottom right - non-growing season

Average annual mean NDVI

Slope of annual mean NDVI

Average growing season mean NDVI

Slope of growing season mean NDVI

Average non-growing season mean NDVI
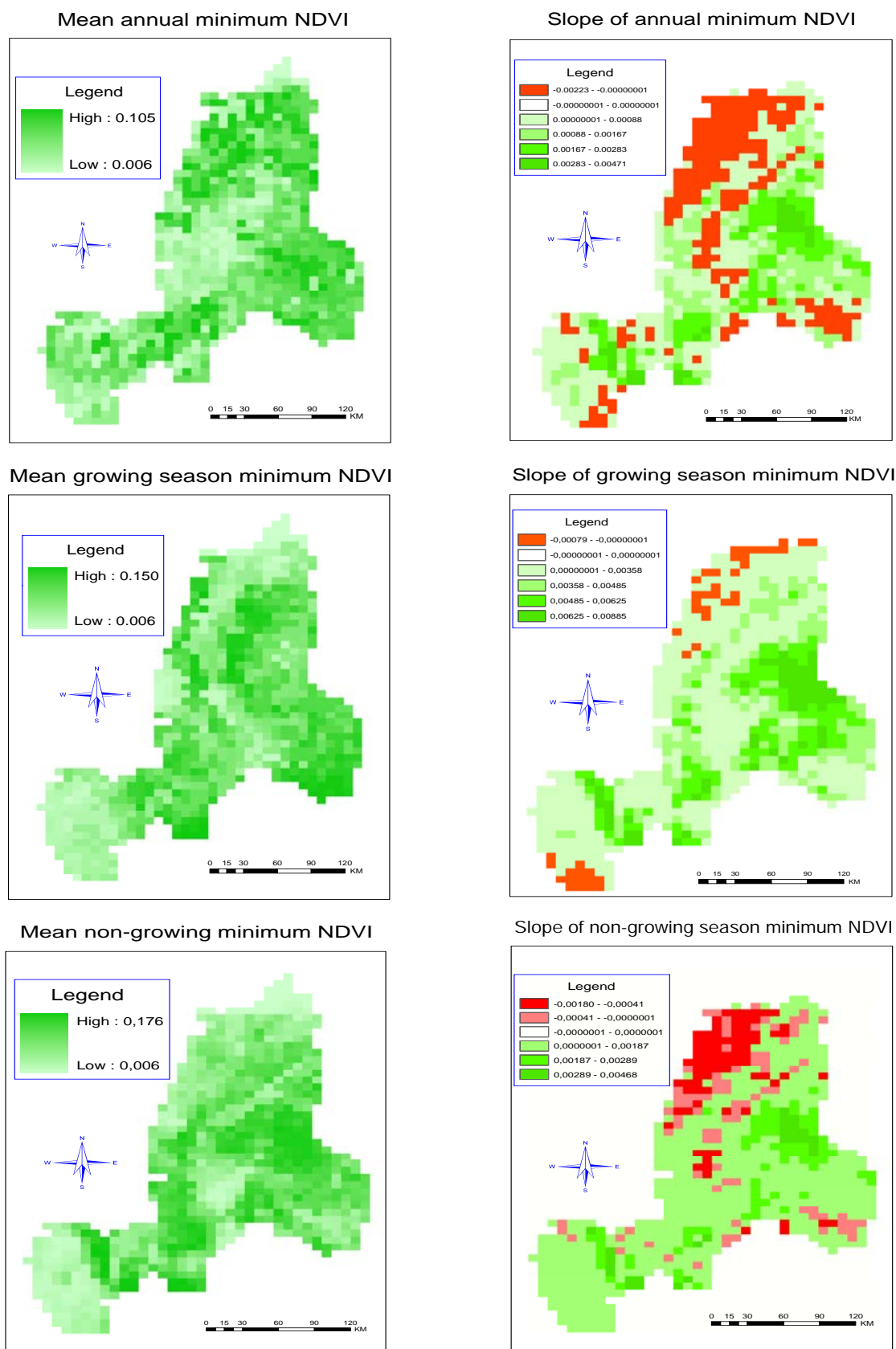
Slope of non-growing season mean NDVI

Figure 8.   Average mean NDVI for 1981-2002: top left - annual; middle left - growing season (May-Oct); bottom left - non-growing season (Nov-Apr). Classified maps of slope coefficients of linear regression for mean NDVI: top right - annual; middle right - growing season; bottom right - non-growing season
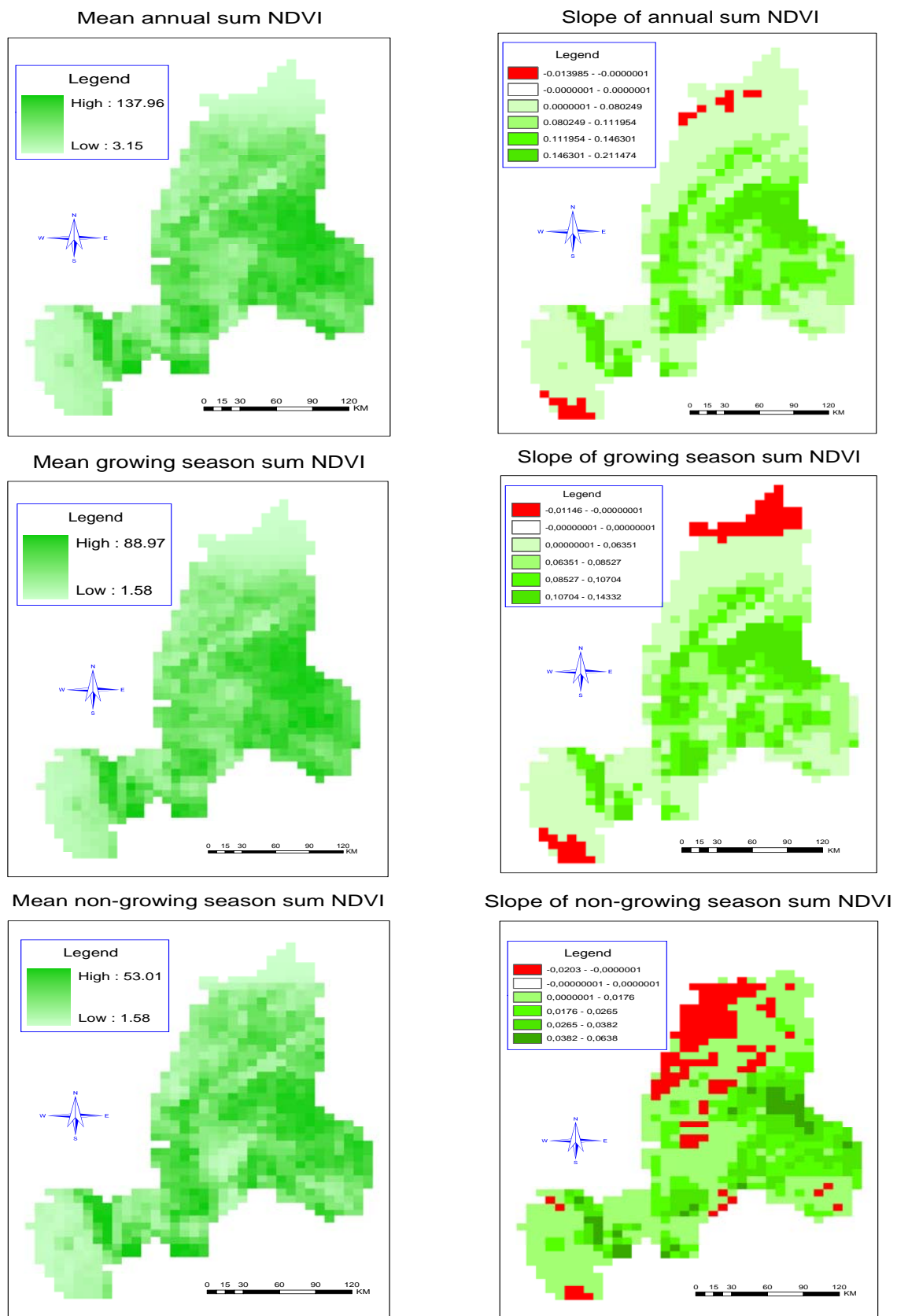
Figure 9.   Mean sum NDVI 1981-2002: top left - annual; middle left - growing season (May-Oct); bottom left - non-growing season (Nov-Apr). Classified maps of slope coefficients of linear regression for sum NDVI: top right - annual; middle right - growing season; bottom right - non-growing season
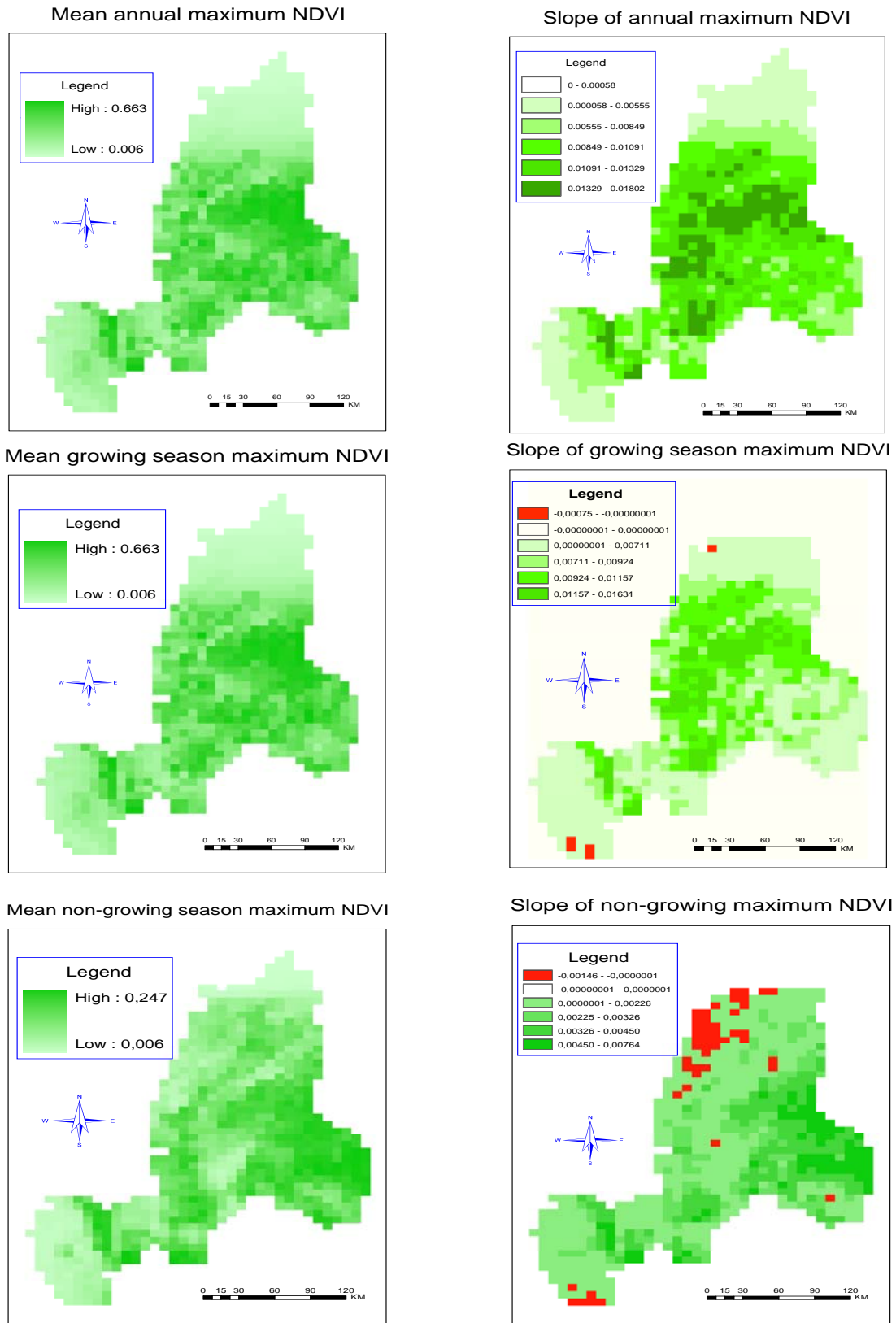
Mean annual NDVI CoV

Slope of annual NDVI CoV

Mean growing season NDVI CoV

Slope of growing season NDVI CoV

Mean non-growing season NDVI CoV

Slope of non-growing season NDVI CoV

Figure 10. Mean NDVI CoV 1981-2002: top left - annual; middle left - growing season (May-Oct); bottom left - non-growing season (Nov-Apr). Classified maps of slope coefficients of linear regression for NDVI CoV: top right - annual; middle right - growing season; bottom right - non-growing season
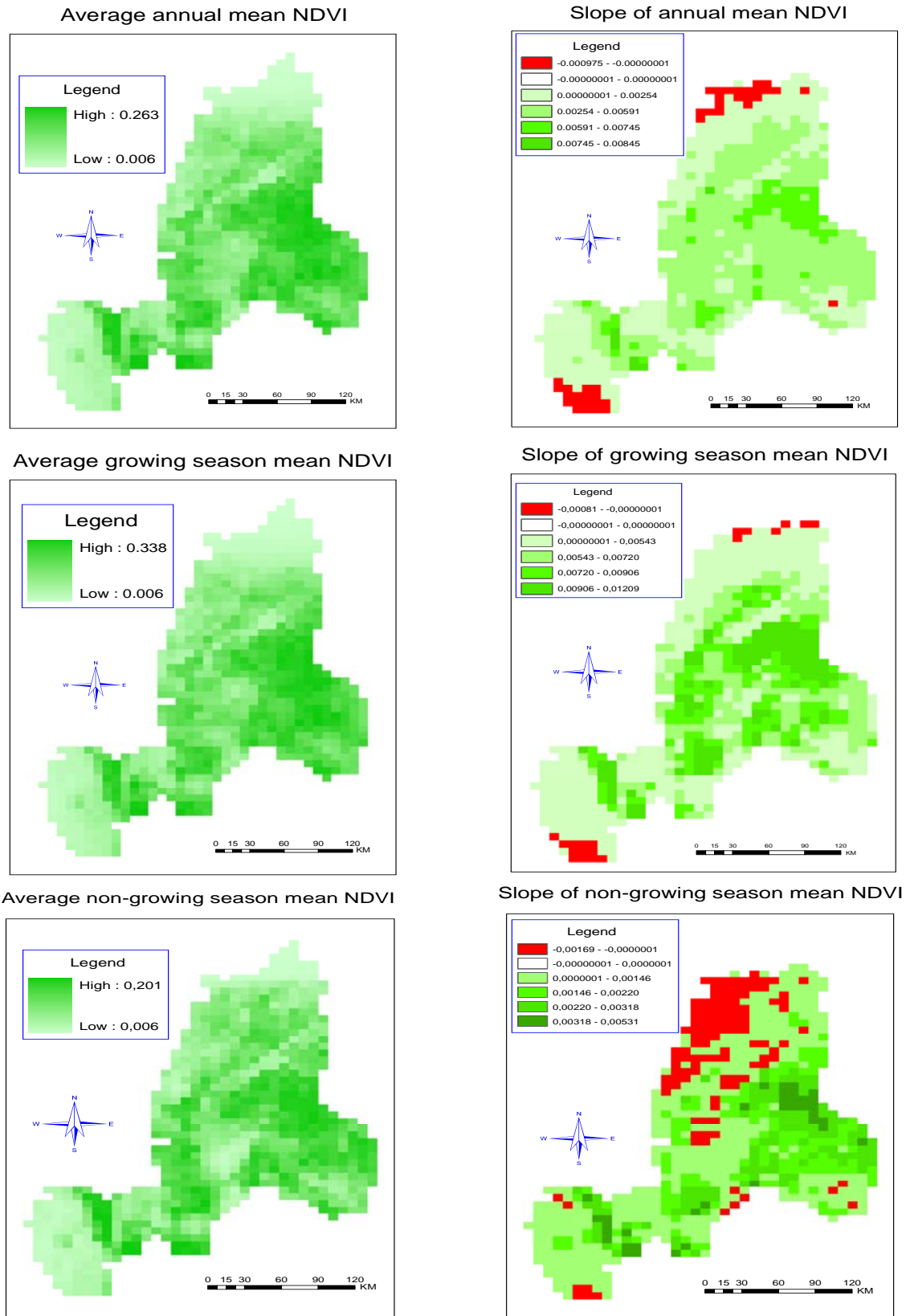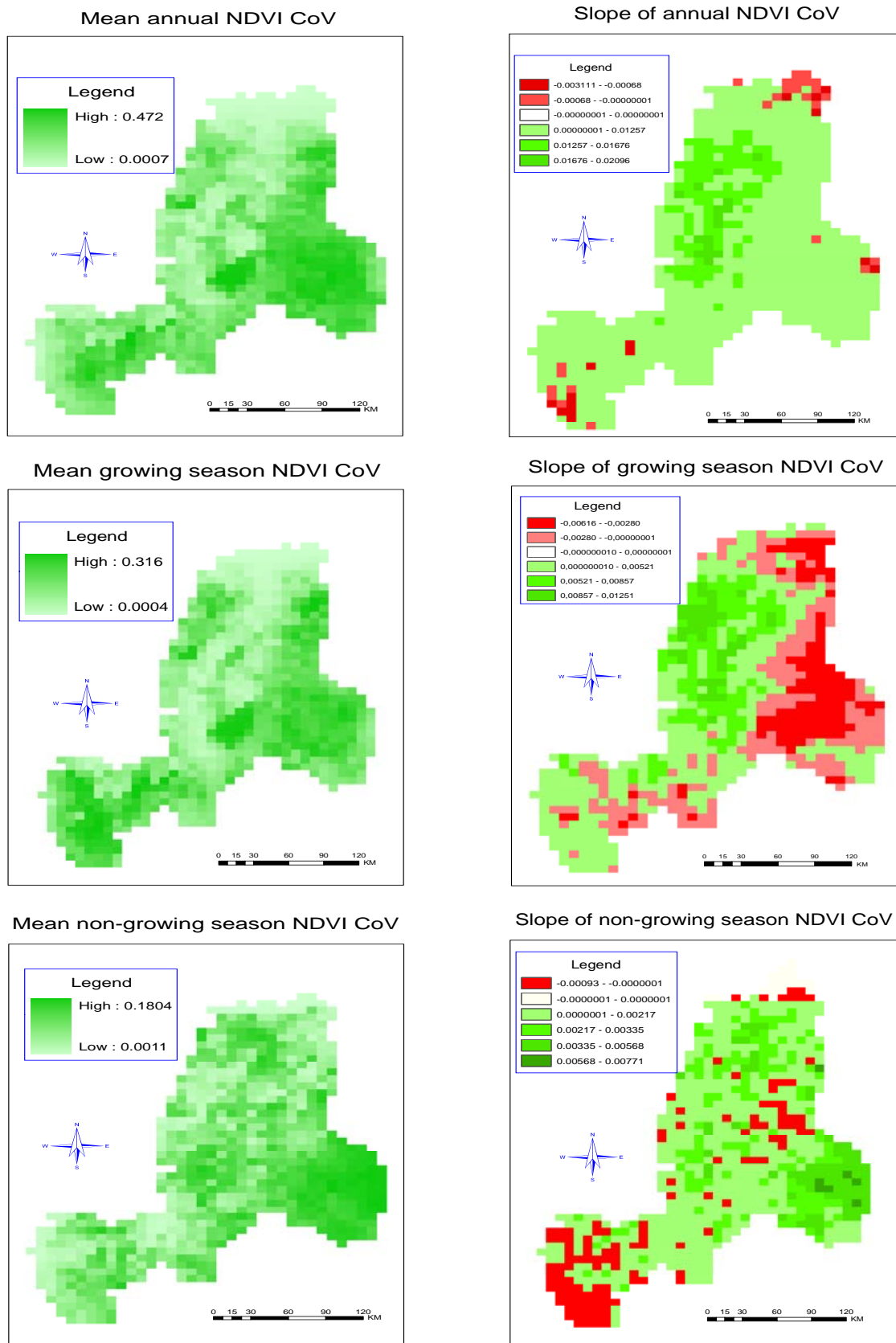
Coefficients of variation (CoV)

CoV can be used to compare the amount of variation in different sets of sample data. It is a dimensionless quantity; all CoV values are at the same scale of magnitude which facilitates comparisons of data collected over different time periods. CoV images were generated by computing for each pixel the standard deviation (STD) of the set of individual NDVI values and dividing this by the mean (M) of these values (CoV = STD/M). This represents the dispersion of NDVI values relative to the mean value over time shown in Fig. 11: 1) positively increasing dispersion, 2) positively decreasing dispersion, 3) negatively decreasing dispersion, and 4) negatively increasing dispersion.

A positive change in the value of a pixel-level CoV over time relates to increased dispersion of values, not increases NDVI; similarly, a negative CoV dispersion means decreasing dispersion of NDVI around mean values, not decreasing NDVI. As an indication of variability, CoV may be combined with other biomass parameters, such as maximum-minimum NDVI, to detect land degradation or improvement (Table 2).

Table 2.   Combination of NDVI and CoV for detection of biomass variation

Max-min NDVI	NDVI CoV	interpretation of biomass variation
+	+	increase + unstable
-	+	decrease + unstable
+	-	increase + stable
-	-	decrease + stable
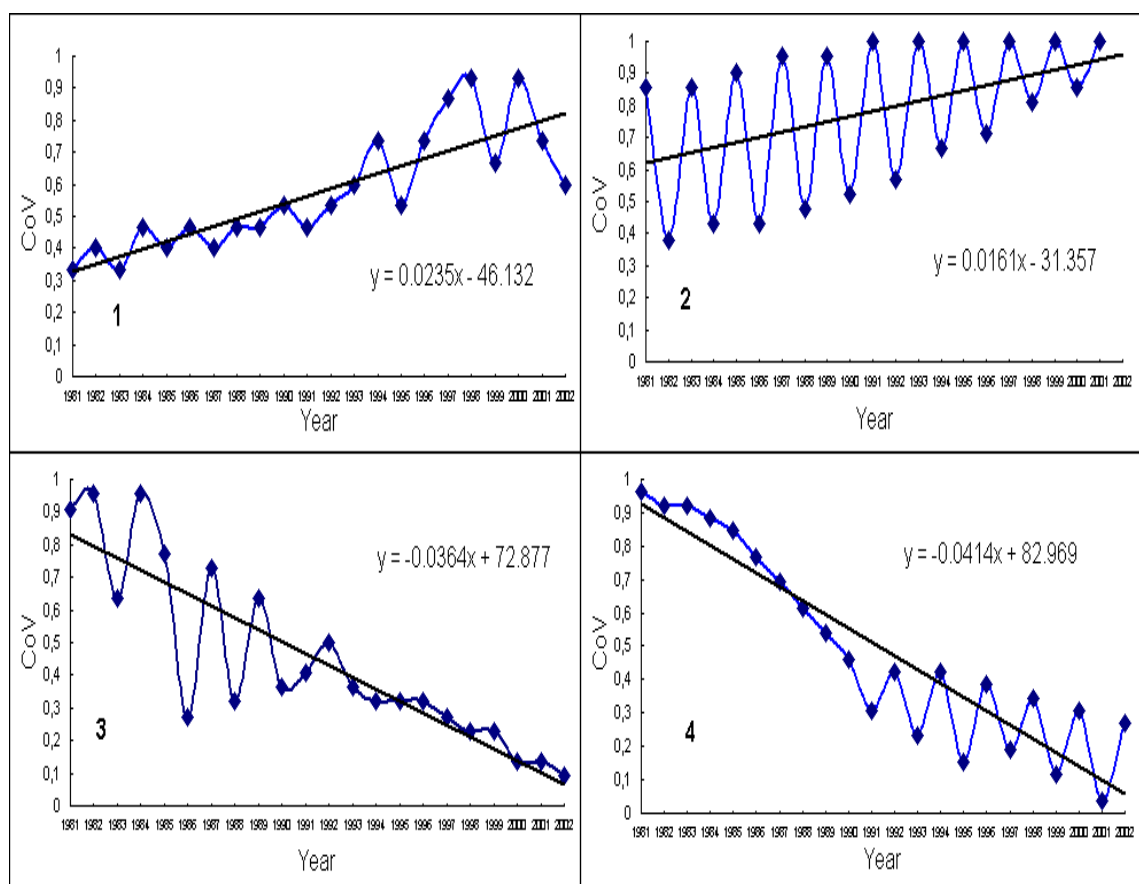
Figure 11. Patterns of NDVI CoV over time

The spatial distribution of average growing season NDVI CoV is similar to the annual NDVI pattern but their temporal trends are quite different: for the growing period, 301 pixels display a negative trend and 454 a positive trend; for the annual period, 37 show a negative trend and 738 a positive. The spatial pattern and trend are different again for the non-growing season (Table 1, Fig. 10).

301 pixels show a negative trend in the growing season NDVI CoV. Of these, only 5 pixels showed a negative trend in the mean NDVI and 296 pixels showed positive trend. These values emphasize that negative trend of CoV does *not* mean biomass decrease, and *vice versa*. Rather, the trends in NDVI CoV may reflect land cover change.

Directly connecting declining values of the NDVI CoV to vegetation or land degradation is incorrect - although several authors have done so, for example Weiss *et al.* (2001), Milich and Weiss (2000), Tucker *et al.* (1991a) and Asner *et al.* (2005).

Interpretation and discussion of NDVI indicators

If land use remains stable, changes in NDVI reflect the trend of green biomass production that may be attributed to land quality, and the success of management in dealing with variables such as climate, pests and disease.

Overall, the green biomass increased in the study period. This can hardly be explained by changes in rainfall or land use:

1. Correlations between annual rainfall and annual maximum NDVI are weak at Yulin and moderate at Dingbian (Table 6) and the trend of rainfall is downwards whereas the trend of NDVI is upwards.
2. For the study area, conversion either from barren land to grassland, grassland to cropland or from agricultural land to built-up land could lead to the decrease in NDVI in the non-growing season and increase in growing season. But only 6.1% of the total area had seen a considerable change in land use - cropland, forest, grassland and urban and/or built-up land have increased by 3.4%, 5.4%, 3.5% and 18.2% respectively; barren land has decreased by 22% (Li *et al.* 2004, Fig. 12).
3. We may also look to changes in grassland and arable management, such as increased application of fertilizer and manure which would increase biomass production. In the context of decreasing rainfall, this may be equated with land improvement.

Distinction needs to be made between land degradation/improvement and land use change; they may be related but they are not the same thing. Evans and Geerken (2004) developed several discriminators between climate-induced and human-induced land degradation depending on annual maximum NDVI. Asner and Heidbrecht (2005) used airborne imaging spectroscopy to measure photosynthetic and senescent canopy cover and bare soil extent; they found that land degradation was associated with a persistent increase in both photosynthetic vegetation (PV) and bare soil, and a lasting decrease in non-photosynthetic vegetation (NPV); there was no change in the spatial variability of PV but its temporal variation decreased substantially. In contrast, degradation was associated with an increase in the spatial variability of NPV, while its temporal variation did not change. Both the spatial and temporal variation of bare soil decreased with land degradation. At the desert margin, desertification appeared to be linked to a decoupling of vegetation responses to inter-annual rainfall variation: higher winter rainfall led to decreased springtime spatial variability in the PV cover; higher summer rainfall resulted in decreased variability in PV cover; the effects of desertification on NPV dynamics were more than three times greater than on PV or bare soil dynamics.

Using remotely sensed PV and NPV as proxies for net primary production (NPP) and litter dynamics, respectively, desertification decreases the temporal variability of NPP and increases spatial variation of litter production and loss.

We should also note the large, recent increase in the exploitation of coal in the north-east and oil in the south-west of the study area. The spatial distribution of the negative trends in mean, max-min and sum NDVI occurred mainly in the northeast and southwest parts of the area.

The results support the previous studies of Gao *et al.* (2001), Zhang *et al.* (2002), Runnström (2000), Runnström *et al.* (2003a, b) but conflicts with Liu (1996) and Liu *et al.* (2003). Yulin prefecture is China's trial area for tackling land degradation and desertification. Progress has been reported in this region in the northern part of the province (*China Daily, 6 September 2001,* http://www.din.net.cn/book2/ctk-12.htm).
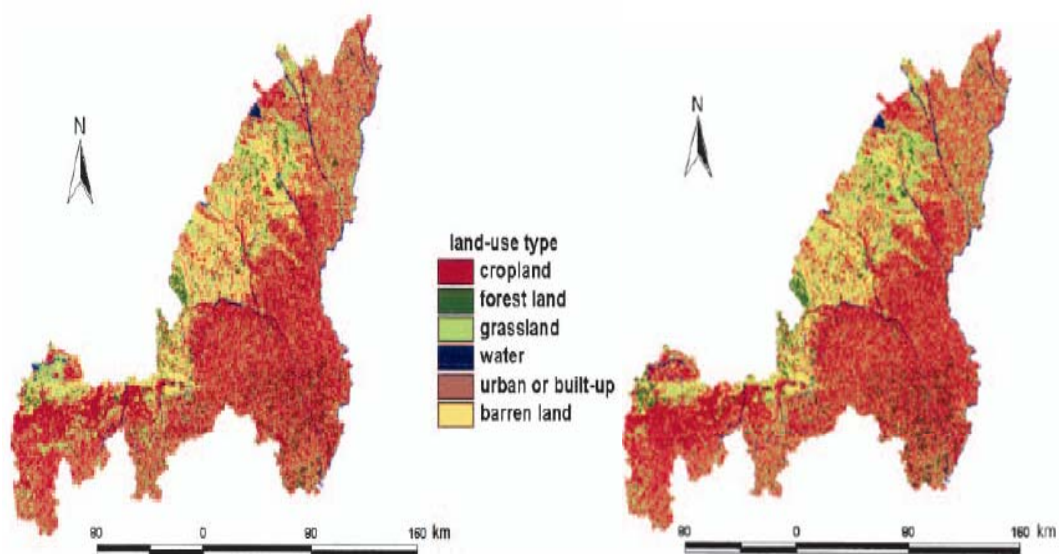
Land-use. Yulin. 1986   Land-use. Yulin. 2000
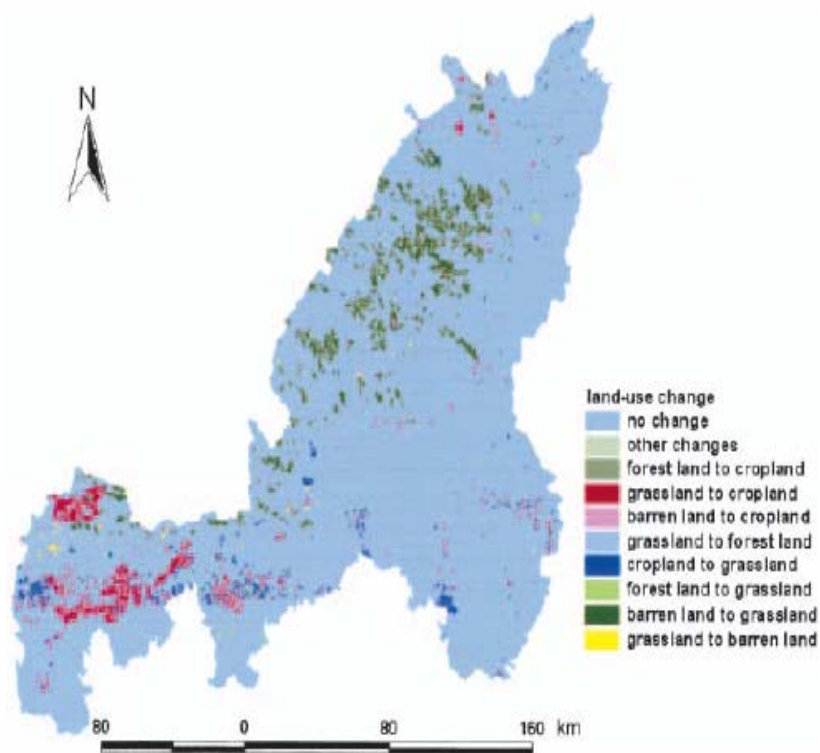

Figure 12. Land use change, Yulin, 1986–2000 (from Li et al. 2004)

4.2   Correlations between NDVI indicators

Correlation coefficients between NDVI coefficients of variation (CoV), mean, minimum, maximum and sum and the slopes of their linear regression equations were queried and statistically analyzed at pixel level (Table 3). The correlations between NDVI CoV, mean, maximum, minimum and sum are moderate, except for the coefficient between mean and sum of NDVI which may be considered alternates. Similar relationships were found for the trends of NDVI indicators over the 22 years period.

Table 3.   Coefficients of variation between NDVI CoV, mean, max, min and sum*

NDVI indicators	Mean v CoV	Mean v Max	Mean v Sum	Mean v Min	CoV v Max	CoV v Sum	CoV v Min	Max v Sum	Max v Min	Sum v Min
NDVI correlation coefficient	0.34	0.66	1.00	0.34	0.65	0.34	0.63	0.66	0.25	0.34
NDVI slope correlation coefficient	0.33	0.72	0.99	0.21	0.74	0.33	0.53	0.72	0.09	0.21

*t-test, n=799; P<0.001

4.3   Biophysical parameters calculated from NDVI for the land degradation types

Average minimum, maximum and mean NDVI of the land degradation levels for each month over time 1981-2002 were queried (Table 4) and their biophysical parameters were calculated according to the SiB land cover reclassification with NDVI-fraction of photosynthetically active radiation absorbed by the canopy (FPAR) scaling values (Defries *et al.* 1998) and ratio vegetation index (RVI) – FPAR relationship (Los *et al.* 2000) (Table 5). There appear to be differences in the range and seasonal trend of NDVI indicators for different degrees of degradation (determined independently of NDVI). This is even more true of the biophysical parameters like rain use efficiency and net primary productivity.

Table 4.   Range of NDVI indicators for different land degradation levels (I-IV)*

Severity level	Indicator	Jan	Feb	Mar	Apr	May	Jun	Jul	Aug	Sep	Oct	Nov	Dec
Severe (I)	Mean NDVI	0.16	0.16	0.17	0.20	0.37	0.38	0.43	0.45	0.39	0.27	0.19	0.16
	Min NDVI	0.14	0.14	0.15	0.17	0.30	0.32	0.37	0.41	0.34	0.23	0.17	0.14
	Max NDVI	0.17	0.18	0.19	0.22	0.41	0.43	0.48	0.49	0.42	0.30	0.20	0.17
High (II)	Mean NDVI	0.17	0.17	0.20	0.28	0.36	0.39	0.44	0.48	0.42	0.31	0.22	0.18
	Min NDVI	0.13	0.13	0.17	0.23	0.30	0.33	0.39	0.44	0.38	0.26	0.18	0.14
	Max NDVI	0.20	0.20	0.24	0.31	0.41	0.46	0.48	0.51	0.47	0.34	0.25	0.22
Medium (III)	Mean NDVI	0.18	0.18	0.19	0.25	0.36	0.44	0.49	0.52	0.47	0.34	0.22	0.18
	Min NDVI	0.13	0.14	0.16	0.20	0.25	0.34	0.42	0.45	0.38	0.27	0.19	0.14
	Max NDVI	0.21	0.21	0.22	0.30	0.46	0.55	0.58	0.58	0.53	0.40	0.25	0.22
Low (IV)	Mean NDVI	0.19	0.18	0.19	0.22	0.32	0.44	0.50	0.51	0.44	0.31	0.21	0.19
	Min NDVI	0.16	0.15	0.17	0.19	0.28	0.39	0.45	0.47	0.35	0.25	0.18	0.16
	Max NDVI	0.20	0.20	0.21	0.24	0.39	0.49	0.54	0.55	0.48	0.34	0.23	0.21

*t-test, n=293, $P < 0.05$ (ref. Dolton *et al.*, 1989; van Reeuwijk and Houba, 1998)

Table 5.   Biophysical parameters calculated from NDVI for the land degradation types

Severity level	$NDVI_{min}$	$NDVI_{mean}$	$NDVI_{max}$	FPAR[1]	RVI[2]	RVC[3](%)	LAIg[4]
Severe (I)	0.14	0.28	0.41	0.392	1.78	7.32	0.86
High (II)	0.13	0.30	0.44	0.417	1.86	9.12	1.24
Medium (III)	0.13	0.32	0.45	0.441	1.94	11.05	2.23
Low (IV)	0.15	0.31	0.47	0.429	1.90	10.07	2.14

1. FPAR = Fraction of Photo-synthetically Active Radiation absorbed by the green leaves of the canopy
2. RVI = Ratio Vegetation Index
3. RVC = Rate of Vegetation Coverage (Purevdorj *et al.* 1998)
4. LAIg = Green Leaf Area Index

4.4 Temporal trends in NDVI according to the severiy of land degradation

Liu *et al.* (2003) combined measurements of vegetation cover, coverage of drifting sand, annual desertification rate and population pressure in a weighted index of land degradation for six counties of the study area. They derived classes I (severe) to IV (low) (Appendix I). Figure 13 shows the trends of the integrated NDVI for their severe to low classes: areas classified as severe (level I) showed decreasing NDVI indicators while others (II-IV) increased over the 22-year period.
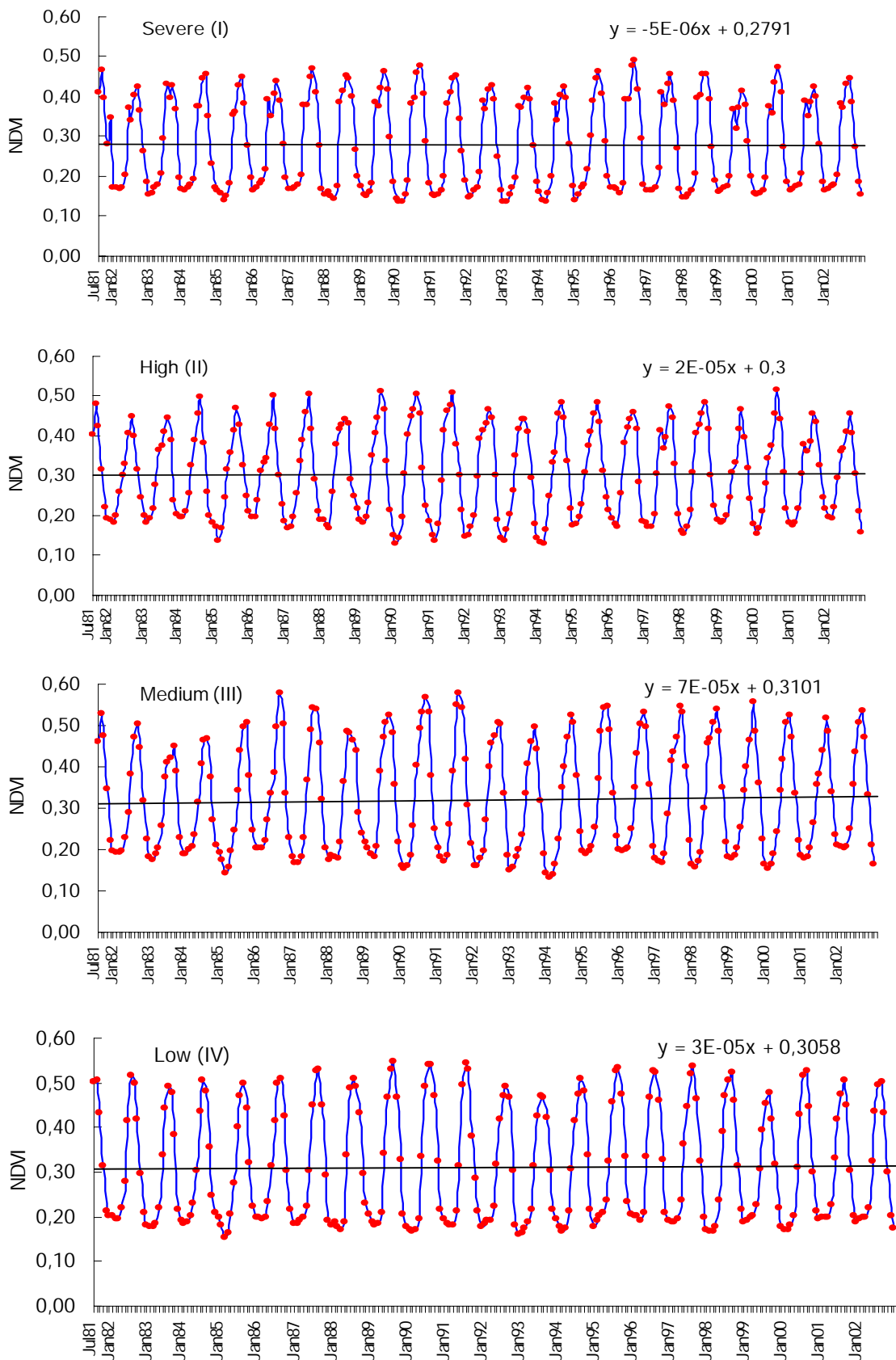
Figure 13. Green-wave (NDVI) for the land degradagtion levels

4.5   Wavelet analysis

Figures 14 shows the patterns of monthly average minimum, maximum and mean NDVI for the different severity levels of land degradation. The gross trends in minimum, maximum and mean NDVI are similar for the various levels of land degradation; they change with local phenology i.e. seeding in May, growth through summer (June-September), and harvest in October. However, comparison of the shapes of the annual NDVI curves (wavelets) with other measures of degradation is revealing: compared with the NDVI wavelet for areas judged not degraded, severely degraded areas show a lower minimum NDVI baseline, delayed onset of growth, and sharply attenuated growth in spring (May), with significantly lower summer production levels.
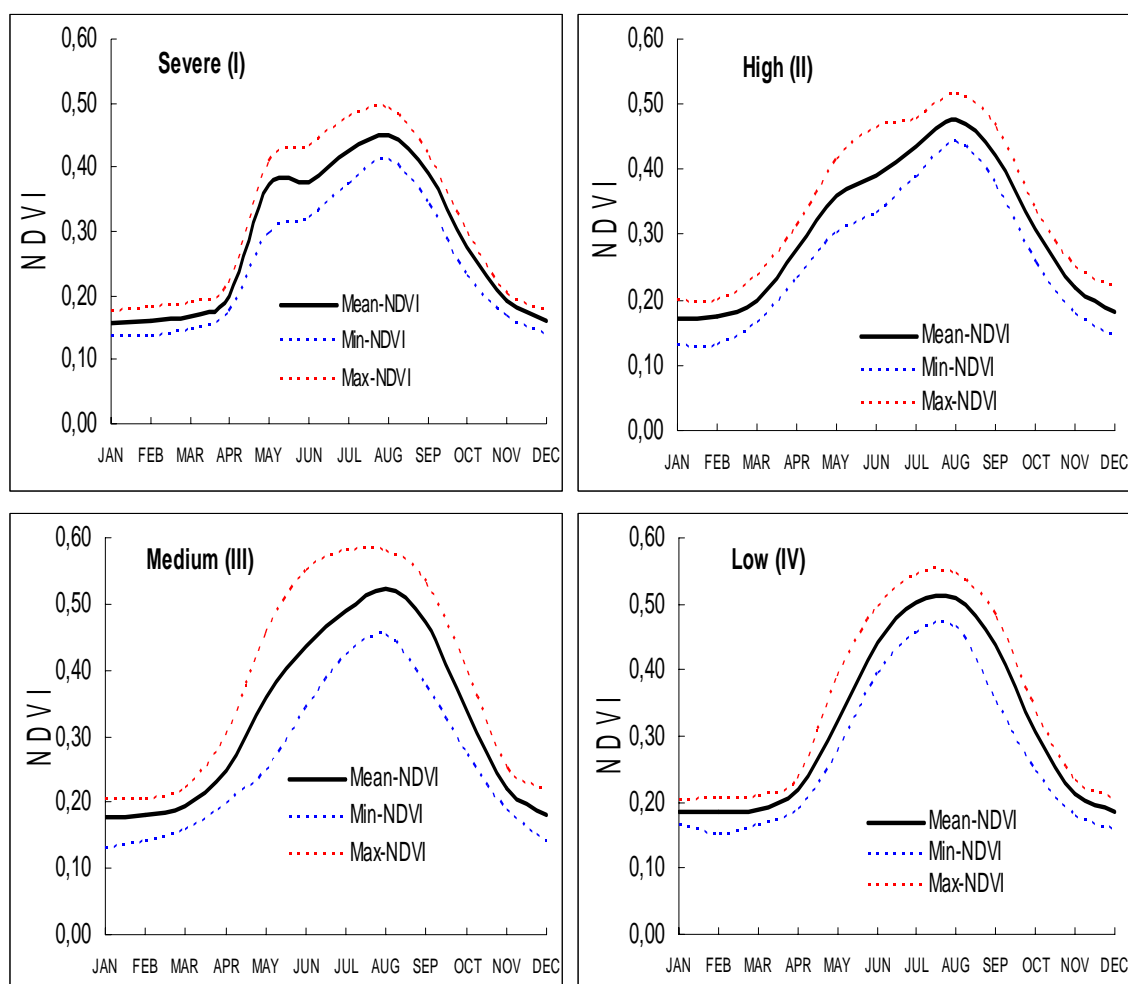
Figure 14. Wavelets of NDVI indicators for different degrees of land degradation

4.6 Trend in yearly integrated NDVI for different degrees of land degradation

Fig. 15 shows trends in yearly integrated NDVI 1981-2002 for different degrees of land degradation. For areas classified as severely degraded, NDVI decreased; while for areas classed as high to low degradation increased (Fig. 15A); the integrated NDVI for the whole study area increased over the 22 years period (Fig. 15B).

Figure 15. Trend in yearly integrated NDVI over time 1981-2002 in the six counties

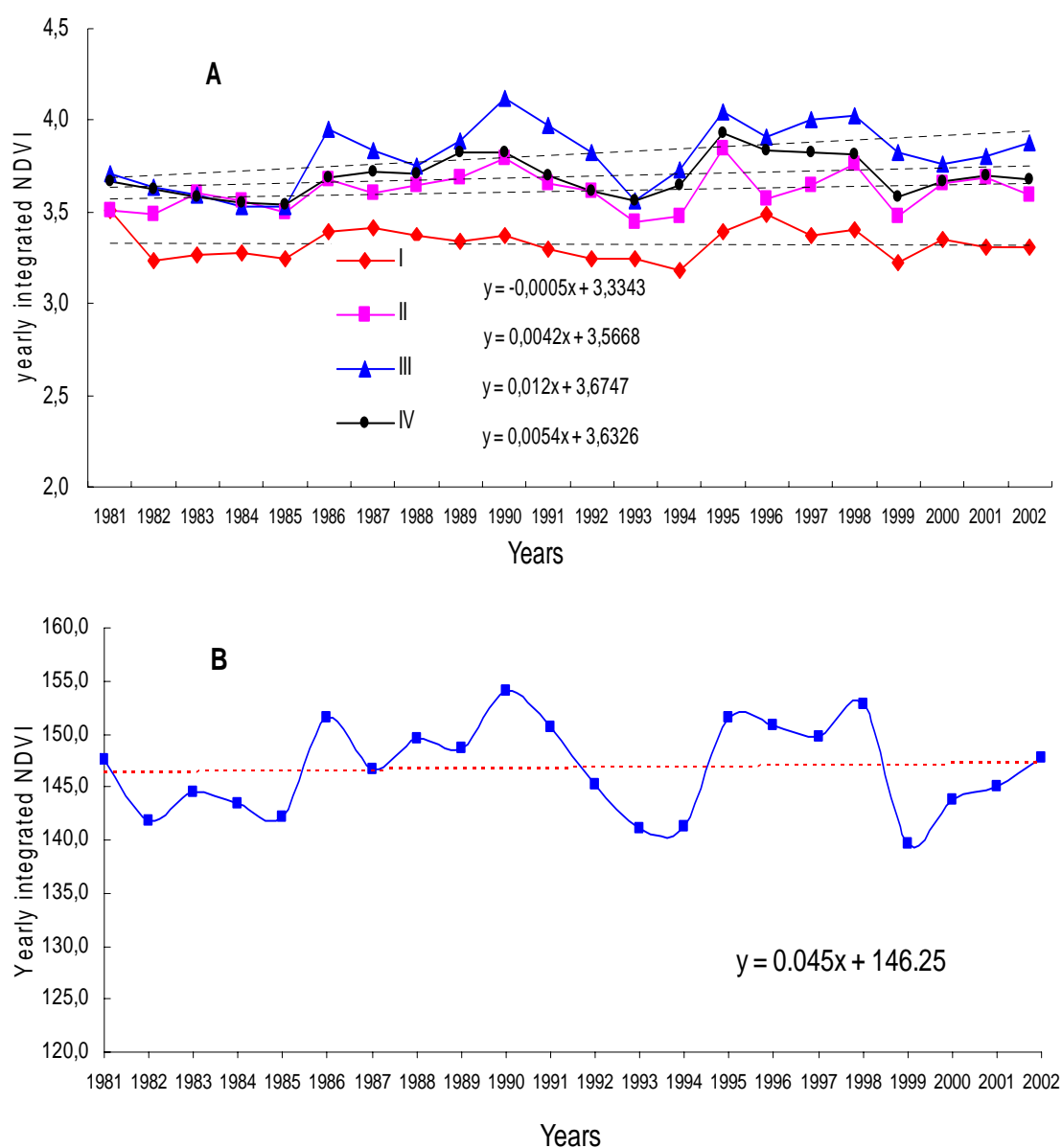## 4.7   Relationships of NDVI with rainfall and temperature

Figure 16 compares trends in annual precipitation with NDVI. Over the 20-year period, rainfall has been decreasing and yet the area as a whole shows increasing green biomass (Fig. 15B). For individual pixels, there may be little or no relation with rainfall (Table 6).

Table 6.   Correlation coefficients between annual rainfall and NDVI indicators

Sites	Rainfall *v* mean NDVI	Rainfall *v* max NDVI	Rainfall *v* min NDVI	Rainfall *v* sum NDVI	Rainfall *v* NDVI CoV
Yulin*	0.049	0.053	0.366	0.049	0.325
Dingbian**	0.644	0.549	0.417	0.504	0.608

*t-test, n=22, P<0.01; ** t-test, n=16, P<0.05

NDVI is strongly correlated with monthly precipitation and temperature; most rain falls during summer growing period – plant growth responding to increasing warmth and moisture in spring and summer (Table 7, Fig. 17).

Table 7.   Correlation coefficients of NDVI with monthly rainfall and temperature

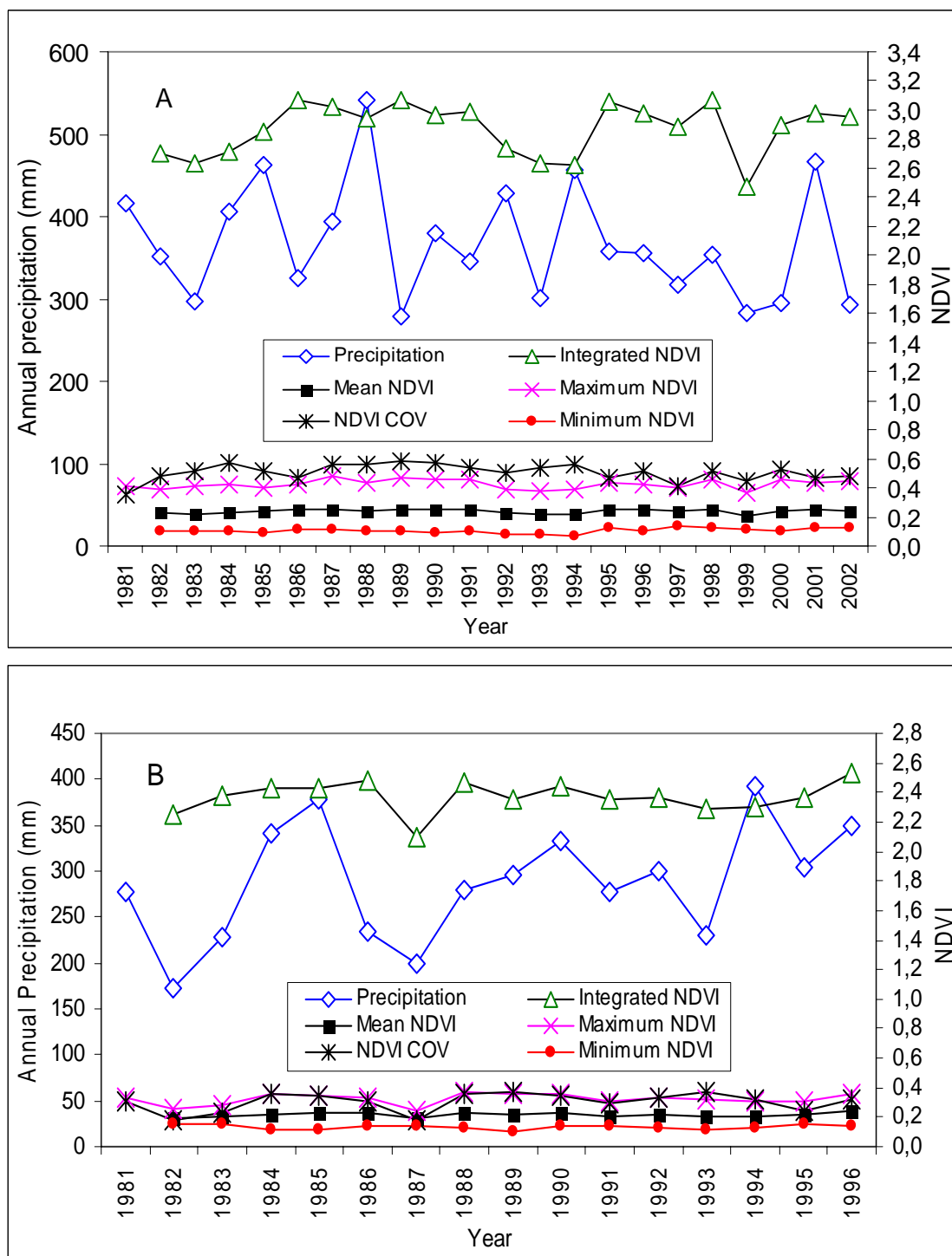| Sites	rainfall *v* NDVI	temperature *v* NDVI
Yulin*	0.607	0.719
Dingbian**	0.618	No data

*t-test: n=257, P<0.001; **t-test: n=192, P<0.001

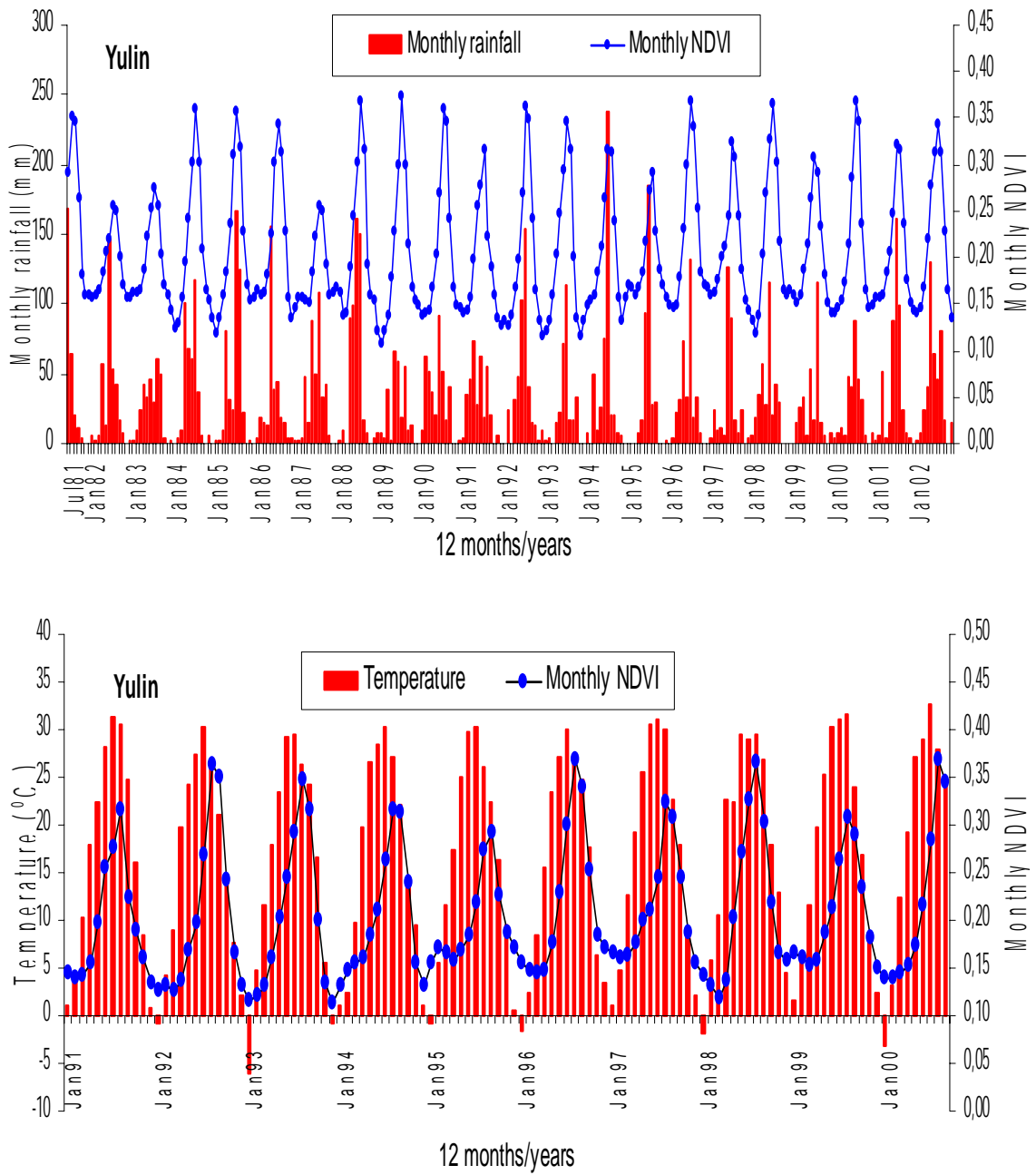Figure 16. Annual rainfall and NDVI at Yulin (A) and Dingbian (B) from 1981 to 1996/2002

Figure 17. Monthly rainfall respectively temperature and NDVI at Yulin

4.8 Relationships between rainfall and NPP

NPP is the net flux of carbon from the atmosphere into a unit area of vegetation per unit time (Schlesinger 1991); it is a key driver of ecological processes so provides a good measure of land degradation (Milton *et al*. 1994, Pickup 1996). Half-monthly NDVI values were summed to monthly NDVI for the same locations as the data from Tao *et al.* (Tao, *personal communication*) to explore the relationship between NPP and NDVI. Linear regression between monthly NPP and NDVI was built as follows:

$$NPP_m \text{ [g C m}^{-2} \text{ month}^{-1}] = 41.691 * \Sigma NDVI_m + 33.192 \qquad [1]$$

where NPP_m is monthly NPP and $\Sigma NDVI_m$ the sum of first and second half-monthly NDVI (n = 1768, r = 0.283, t-test P<0.001)

Then growing-season and yearly sums of NPP and NDVI were integrated. The resulting relationships are:

$$NPP_{May-Oct} \text{ [g C m}^{-2} \text{ (May-Oct)}^{-1}] = 13.78 * \Sigma NDVI_{May-Oct} + 281.5 \quad [2]$$

where $NPP_{May-Oct}$ is the summation of NPP between May and October, $\Sigma NDVI_{May-Oct}$ is the integrated NDVI for May-October (n = 303, r = 0.18, t-test P<0.001) and

$$NPP_a \text{ [g C m}^{-2} \text{ yr}^{-1}] = 0.0349 * \Sigma NDVI + 294.85 \qquad [3]$$

where NPP_a is the annual sum of NPP; $\Sigma NDVI$ the annual NDVI
(n = 303, r = 0.18, t-test P<0.001)

The monthly rainfall data for Yulin and Dingbian were taken to link NPP to NDVI (Table 8). There are fairly poor agreements between model-based NPP and remotely-sensed estimates of the total green biomass (NDVI) for annual time intervals but better at monthly intervals; NPP seems to be in step with monthly rainfall with no significant time lag.

The trend in NPP over time in the area, as a whole, increased (Fig. 18).

Table 8.   Correlations of NPP with NDVI and precipitation at Yulin and Dingbian*

| Parameters	Time intervals	Yulin	Dingbian
NPP-NDVI	Yearly	NPP=4.0696NDVI+300 r=0.09, n=18	NPP=44.362NDVI+87.013 r=0.381, n=16
	May-October	NPP=3.5355NDVI+284.48 r=0.066, n=18	NPP=32.752NDVI+155.13 r=0.315, n=16
	Monthly	NPP=28.621NDVI+32.406 r=0.253, n=104	NPP=49.644NDVI+20.621 r=0.273, n=94
NPP- Precipitation	Yearly	NPP=0.8327Preci+8.9674 r=0.66, n=18	NPP=0.3231Preci+165.89 r=0.44, n=16
	May-October	NPP=0.742Preci+52.976 r=0.73, n=18	NPP=0.3121Preci+158.77 r=0.46, n=16
	Monthly	NPP=0.3204Preci+32.852 r=0.51, n=104	NPP=0.3009Preci+26.779 r=0.50, n=94
	Monthly (1 month lag of NPP)	NPP=0.0756Preci+45.598 r=0.038, n=103	NPP=0.0532Preci+37.115 r=0.087, n=93

* t-test; $P < 0.001$
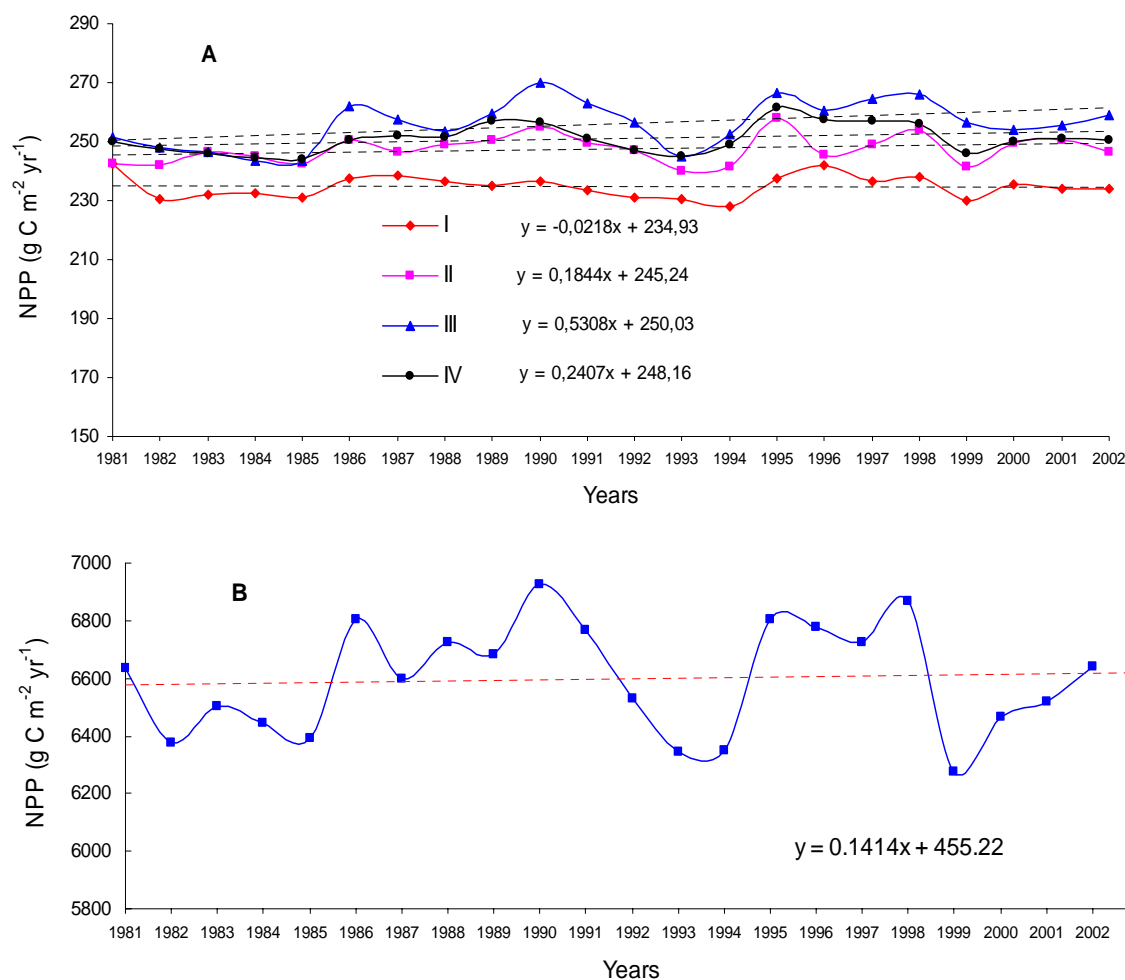
Figure 18. Temporal trends in net primary productivity (1981-2002)

4.9 Rain-use efficiency

A reduction in NDVI does not necessarily indicate land degradation; green biomass also fluctuates between and within years according to phenology, variation in rainfall, and changes in land use – all of which may be unrelated to the land degradation. Similarly, NPP may not serve as an indicator of land degradation without taking the rainfall into account.

Rain-use efficiency (RUE) – the ratio of NPP to precipitation – seeks to overcome this problem by combining information on biomass production and rainfall (Prince *et al*. 1998, Nicholson *et al*. 1998). RUE tends to decrease when aridity and potential evapotranspiration increase; it has also been shown that RUE is lower in degraded arid lands than in equivalent un-

degraded areas (Le Houerou 1984). Negative deviations from the conservative value of RUE may provide a useful index of land degradation.

Temporal trends in RUE, computed as the ratio between NPP and rainfall (hereafter referred to as RUE_{NPP}) and ratio between NDVI and rainfall (hereafter referred to as RUE_{NDVI}), increased at Yulin and decreased at Dingbian (Fig. 19). This suggests land improvement at Yulin and degradation at Dingbian; Yulin has taken counter-measures against desertification such as increasing vegetation cover through aerial seeding, direct planting, sand dune stabilization, fencing and shelterbelt systems for farmland and pasture (Wu *et al.* 1997, Zhu and Wang 1993). In the Dingbian area, in contrast, the oil industry has encroached upon grassland and cropland.
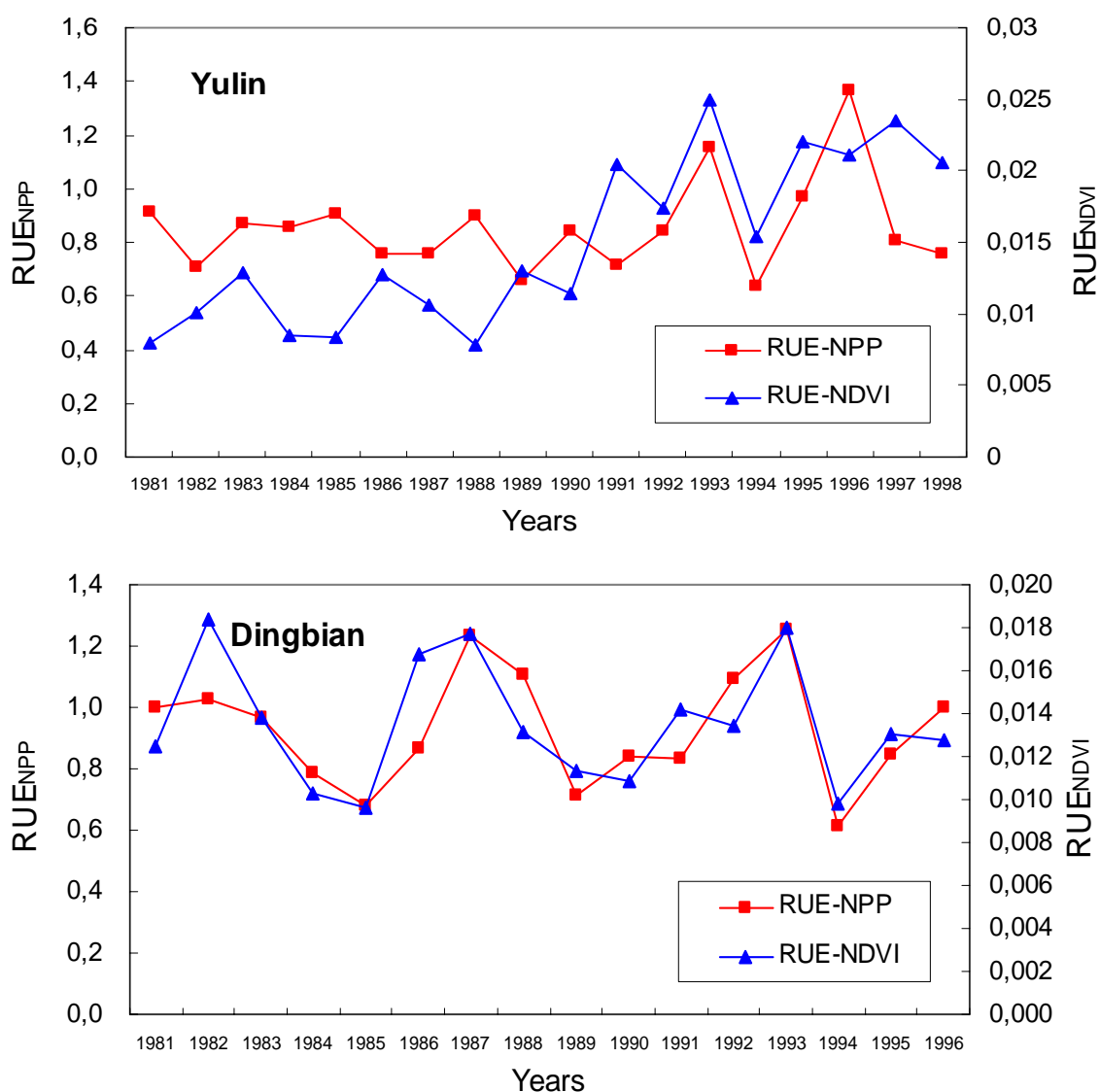
Figure 19. Trends in rain-use efficiency

The correlation between RUE_{NPP} and RUE_{NDVI} at annual intervals is significant with correlation coefficients of 0.33 at Yulin (n=18, t-test P<0.01) and 0.74 at Dingbian (n=16, t-test P<0.01), respectively (Fig. 20); and higher at monthly intervals: r=0.81 at Yulin (n=104, t-test P<0.01); and r=0.74 at Dingbian (n=94, t-test P<0.01)(Fig. 21), so NDVI could be used as a proxy for NPP.

Figure 20. Relationships of RUE_{NPP} with RUE_{NDVI} at annual intervals

Figure 21. Relationships of RUE$_{NPP}$ with RUE$_{NDVI}$ at monthly intervals

5. SUMMARY AND CONCLUSIONS

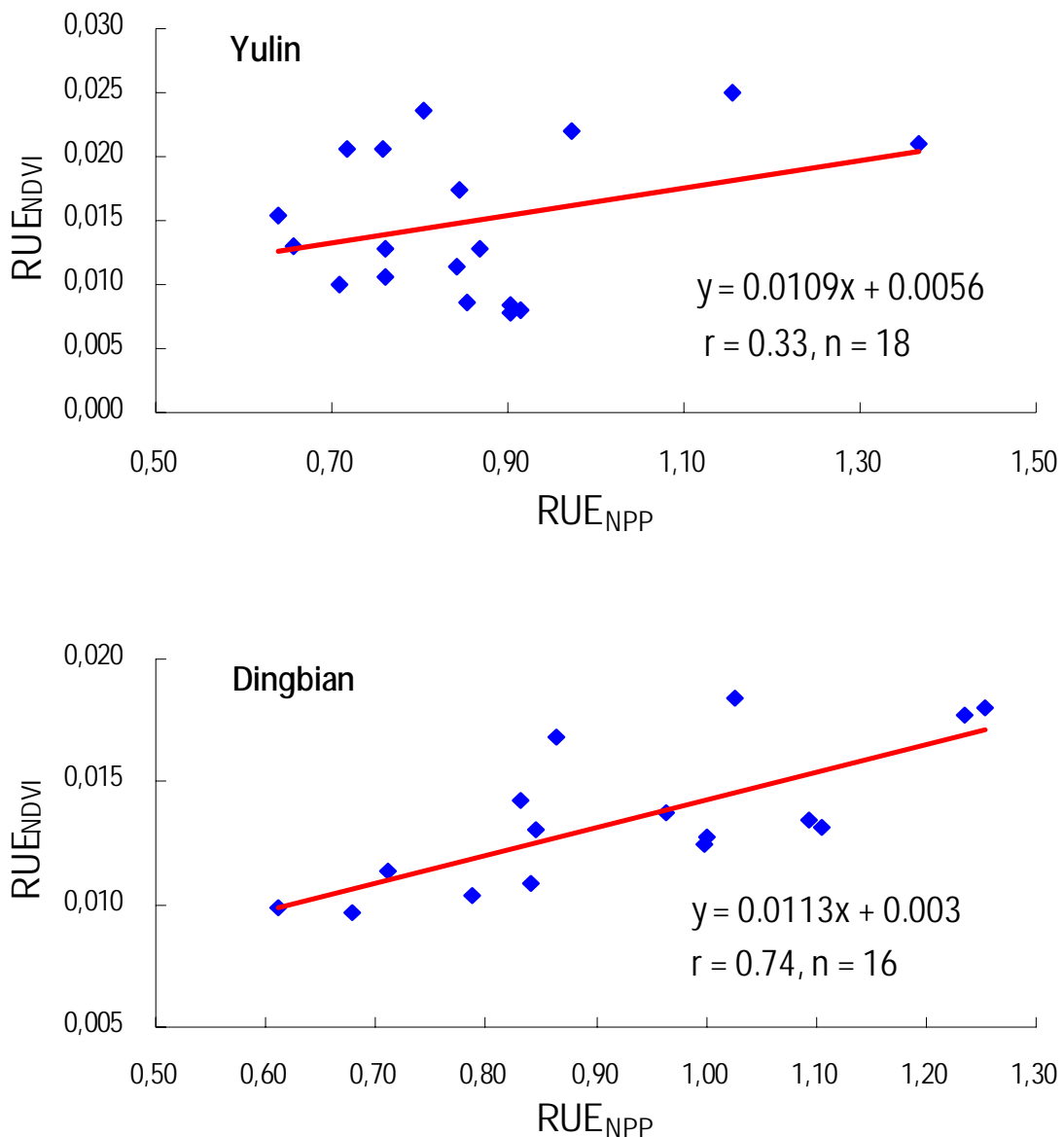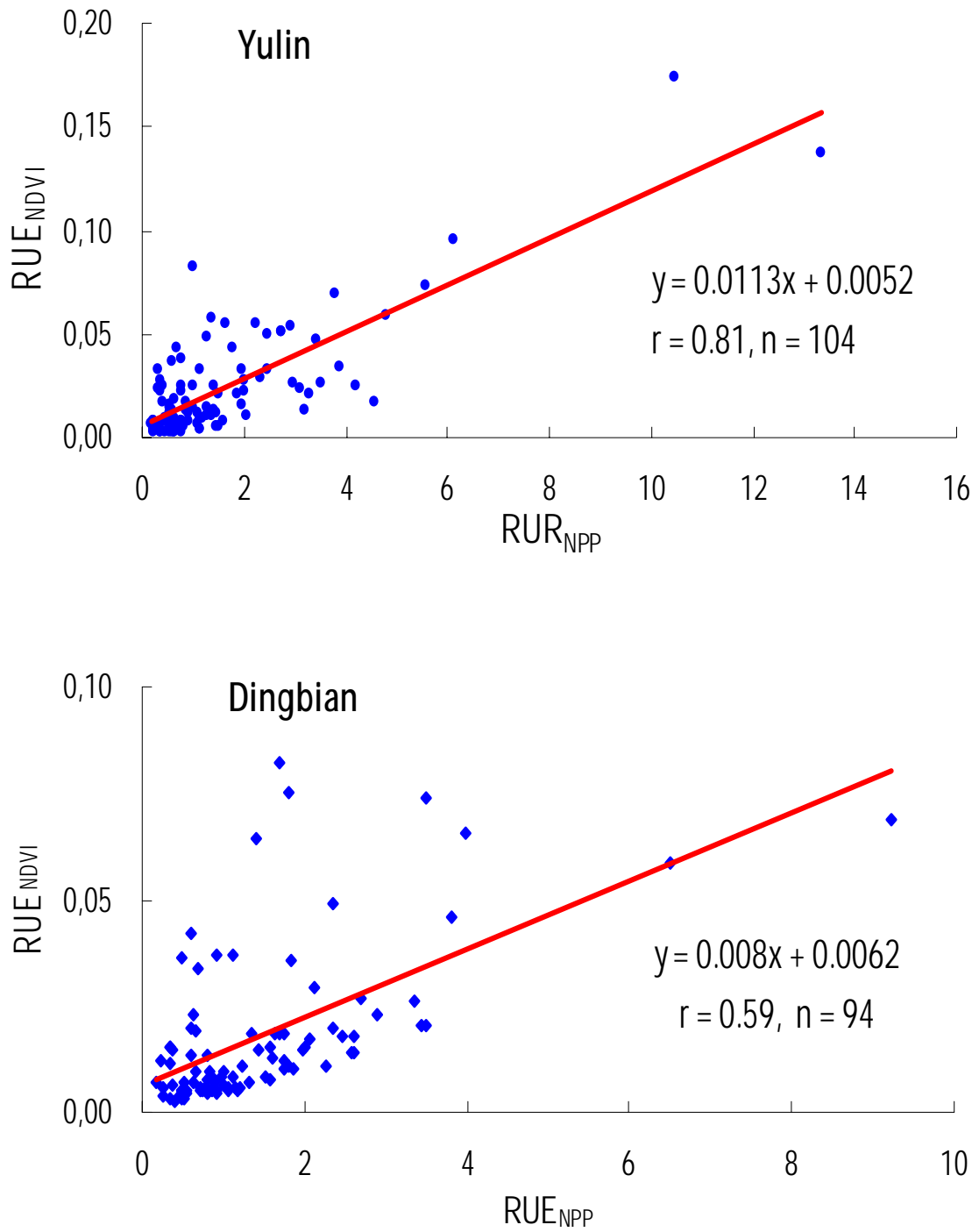- All NDVI indicators have biological meaning. Their temporal trends can be indicated by the slope of the linear regression equation. NDVI CoV, however, cannot be used to directly reflect trends in green biomass change; it should be combined with other indicators for detection of biomass degradation or improvement.

- Correlations of the NDVI indicators and net primary productivity (NPP) with annual rainfall are low to moderate, but higher with monthly rainfall. Rain-use efficiency, both computed as the ratio between NPP and rainfall (RUE_{NPP}) and as ratio between NDVI and rainfall (RUE_{NDVI}), increased at Yulin and slightly decreased at Dingbian. The correlations between RUE_{NPP} and RUE_{NDVI} are statistically significant, and higher at the monthly intervals, they can be alternates.

- Analyses of average annual, growing season and non-growing season NDVI indicators and their temporal trends indicate that the green biomass, overall, increased over the 22-year period without close correspondence with rainfall. Signs of declining green biomass production, which may indicate active land degradation, are localised. This result supports the previous studies of Gao *et al.* (2001), Zhang *et al* (2002), Runnström (2000) and Runnström *et al.* (2003), but conflicts with Liu *et al.* (2003).

- This study has not considered whether the increase in green biomass, expressed as NDVI, has improved the land quality. However, increased vegetation cover would protect and bind the soil and, thus, decrease soil erosion potential and lead to increase in soil organic matter.

- The indices developed here can be used as an input in early warning systems of land degradation or land improvement – once they are validated by field study.

6. OUTLOOK

The objective of this study was to develop a methodology for assessment of land degradation and land improvement using AVHRR NDVI. The statistical approach was aimed at analysis of spatiotemporal trends in green biomass. The modelling approach was based on data modelling and statistical analysis aiming at managing data and determining the proper green biomass (NDVI) parameters - rather than analyzing long-term spatial changes. Both methods are useful for handling and displaying large datasets.

Two methods that are yet to be fully explored are:

1. ArisFlow which may have application to convert and analyse the GIMMS NDVI datasets (NDVI images, latitude image and longitude image) and clip the NDVI images of the study area from the processed GIMMS datasets (Eurasian continent).
2. HANTS (Harmonic Analyses of NDVI Time-Series) algorithm, to smooth and reconstruct the GIMMS NDVI time-series and remove extreme values that could affect the generalization of processing NDVI time-series.

The next step in analysis of the remotely sensed data will be to stratify the study area according to soil and terrain (SOTER) units and land use, to calculate deviation of the NDVI indicators from local means. By comparing like with like, land degradation hotspots – and areas where degradation has been arrested or reversed - may be identified with greater confidence.

REFERENCES

Archer ERM 2004. Beyond the "climate versus grazing" impasse: using remote sensing to investigate the effects of grazing system choice on vegetation cover in the eastern Karoo. *Journal of Arid Environments* 57, 3, 381–408

Asner GP, Elmore AJ, Olander LP, Martin RE and Harris AT 2004. Grazing systems and global change. *Annual Reviews of Environment and Resources* 29, 261–299

Asner GP and Heidebrecht KB 2005. Desertification alters regional ecosystem-climate interactions. *Global Change Biology* 11, 1, 182-194

Asner GP, Borghi CE and Ojeda RA 2003. Desertification in central Argentina: changes in ecosystem carbon and nitrogen from imaging spectroscopy. *Ecological Application* 13, 4, 629–648

Asrar GM, Fuchs M, Kanemasu ET and Hatfield JL 1984. Estimating absorbed photosynthetically active radiation and leaf area index from spectral reflectance in wheat. *Agronomy Journal* 87, 300–306

Bastin GN, Pickup G and Pearce G 1995. Utility of AVHRR data for land degradation assessment—a case study. *International Journal of Remote Sensing* 16, 4, 651-672

Bradley BA and Mustard JF 2005. Identifying land cover variability distinct from land cover change: Cheatgrass in the Great Basin. *Remote Sensing of Environment* 94, 2, 204–213

Budde ME, Tappan G, Rowland J, Lewis J and Tieszen LL 2004. Assessing land cover performance in Senegal, West Africa using 1-km integrated NDVI and local variance analysis. *Journal of Arid Environments* 59, 3, 481–498

Cao Mingkai and Woodward F Ian 1998a. Dynamic responses of terrestrial ecosystem carbon cycling to global climate change. *Nature* 393, 249-252

Cao Mingkai and Woodward F Ian 1998b. Net primary and ecosystem production and carbon stocks of terrestrial ecosystems and their responses to climate change. *Global Change Biology* 4, 185-198

Defries RS, Hansen M, Townshend JRG and Solberg R 1998. Global land cover classification at 8 km spatial resolution: the use of training data derived from Landsat imagery in decision tree classifiers. *International Journal of Remote Sensing* 19, 16, 3141–3168

Diouf A and Lambin EF 2001. Monitoring land-cover changes in semi-arid regions: remote sensing data and field observations in the Ferlo, Senegal. *Journal of Arid Environments* 48, 2, 129–148

Dolton PJ, Makepeace GH and Treble JG 1989. Statistics in action. Book 1: Descriptive statistics. Published by McGRAW-HILL Book Company (UK) Limited

Dregne HE, Kassas M and Rozanov B 1991. A new assessment of the world status of desertification. *Desertification Control Bulletin* 20, 6–19

Evans J and Geerken R 2004. Discrimination between climate and human-induced dryland degradation. *Journal of Arid Environments* 57, 4, 535-554

Gao J, Zha Y and Ni S 2001. Assessment of the effectiveness of desertification rehabilitation measures in Yulin, north-western China using remote sensing. *International Journal of Remote Sensing* 22, 18, 3783-3795

Geerken R and Ilaiwi M 2004. Assessment of rangeland degradation and development of a strategy for rehabilitation. *Remote Sensing of Environment* 90, 4, 490-504

Hochschild V, Marker M, Rodolfi G and Staudenrausch H 2003. Delineation of erosion classes in semi-arid Southern African grasslands using vegetation indices from optical remote sensing data. *Hydrological Processes* 17, 5, 917-928

Holm AM, Cridland SW and Roderick ML 2003. The use of time-integrated NOAA NDVI data and rainfall to assess landscape degradation in the arid shrubland of Western Australia. *Remote Sensing of Environment* 85, 2, 145–158

IGBP Terrestrial Carbon Working Group 1998. The terrestrial carbon cycle: implications for the Kyoto Protocol. *Science 280,* 1393-1394

Le Houerou HN 1984. Rain-use efficiency: a unifying concept in arid-land ecology. *Journal of Arid Environments* 7, 213–247

Li J, Lewis J, Rowland J, Tappan G. and Tieszen LL 2004. Evaluation of land performance in Senegal using multi-temporal NDVI and rainfall series. *Journal of Arid Environments* 59, 3, 463-480

Li Y 1998. Land degradation: Its social economic dimensions, *China Environmental Sciences* 18, 92–97 (supplement)

Li Z, Li X, Wang Y, Ma A and Wang J 2004. Land-use change analysis in Yulin prefecture, north-western China using remote sensing and GIS. *International Journal of Remote Sensing* 25, 24, 5691–5703

Liu YS and Gao Yay 2002. Assessment and current analysis of land degradation along the Great Wall in northern Shaanxi Province. *Acta Geographica Sinica* 57, 4, 443-450

Liu YS, Gao Jay and Yang Yanfeng 2003. A holistic approach towards assessment of severity of land degradation along the Great Wall in northern Shaanxi Province, China. *Environmental Monitoring and Assessment* 82, 2, 187–202

Liu YS 1996. A remote sensing and GIS integrated study on spatial optimal allocation of regional land use. *Journal of Nanjing Normal University* 19, 90–96 (supplement)

Los SO, Collatz GJ, Sellers PJ, Malmstrom CM, Pollack NH, Defries RS, Bounoua L, Parris MT, Tucker CJ and Dazlich DA 2000. A global 9-year biophysical land surface dataset from NOAA AVHRR data. *Journal of Hydrometeorology* 1, 183–199

Maselli F, Gilabert MA and Conese C 1998. Integration of High and Low Resolution NDVI Data for Monitoring Vegetation in Mediterranean Environments. *Remote Sensing of Environment* 63, 3, 208-218

Maselli F, Romanelli S, Bottai L and Zipoli G 2003. Use of NOAA-AVHRR NDVI images for the estimation of dynamic fire risk in Mediterranean areas. *Remote Sensing of Environment* 86, 2, 187–197

Millch L and Weiss E 2000. GAC NDVI interannual coefficient of variation (CoV) images: ground truth sampling of the Sahel along north-south transects. *International Journal of Remote Sensing* 21, 2, 235-260

Milton SJ, Dean WRJ, du Plessis MA and Siegfried SWR 1994. A conceptual model of arid rangeland degradation: the escalating cost of declining productivity. *Bioscience 44,* 70-76

Mouat D, Lancaster J, Wade T, Wickham J, Fox C, Kepner W and Ball T 1997. Desertification evaluated using an integrated environmental assessment model. *Environmental Monitoring and Assessment* 48, 2, 139–156

Myneni RB, Keeling CD, Tucker CJ, Asrar G and Nemani RR 1997. Increased plant growth in the northern high latitudes from 1981 to 1991. *Nature* 386, 698-702

Nicholson SE, Tucker CJ and Ba MB 1998. Desertification, drought, and surface vegetation. An example from the West African Sahel. *Bulletin of the American Meteorological Society* 79, 5, 815-829

Oldeman LR, Hakkeling RTA and Sombroek WG 1991. World map of the status of human-induced soil degradation: an explanatory note, second revised edition. ISRIC, Wageningen, and UNEP, Nairobi

Paruelo JM, Epstein HE, Lauenroth WK and Burke IC 1997. ANPP estimates from NDVI for the central grassland region of the United States. *Ecology* 78, 3, 953-958

Pelkey NW, Stoner CJ, Caro TM 2000. Vegetation in Tanzania: assessing long term trends and effects of protection using satellite imagery. *Biological Conservation* 94, 3, 297-309

Pickup G 1996. Estimating the effects of land degradation and rainfall variation on productivity in rangelands: an approach using remote sensing and models of grazing and herbage dynamics. *Journal of Applied Ecology* 33, 4, 819-832

Potter CS, Randerson JT, Field CB, Matson PA, Vitousek PM, Mooney HA and Klooster SA 1993. Terrestrial ecosystem production: a process model based on global satellite and surface data. *Global Biogeochemical Cycles* 7, 4, 811–841

Prince SD, Brown de Colstoun E and Kravitz L 1998. Evidence from rain-use efficiencies does not indicate extensive Sahelian desertification. *Global Change Biology* 4, 4, 359-374

Purevdoj Ts, Tateishi R, Ishiyama T and Honda Y 1998. Relationships between percentage vegetation cover and vegetation indices. *International Journal of Remote Sensing* 19, 18, 3519-3535

Reeuwijk van LP and Houba VJG 1998. Guidelines for quality management in soil and plant laboratories. FAO SOILS BULLETIN, 74

Reynolds JF and Stafford Smith M 2002. Do humans create deserts? In: Global desertification. Do humans create deserts? (pp.1–22). Berlin: Dahlem University Press

Ringrose S, Vanderpost C and Matheson W 1996. The use of integrated remotely sensed and GIS data to determine causes of vegetation cover change in southern Botswana. *Applied Geography* 16, 3, 225-242

Running SW and Nemani RR 1988. Relating seasonal patterns of the AVHRR vegetation index to simulated photosynthesis and transpiration of forests in different climates. *Remote Sensing of Environment* 24, 2, 347– 367

Runnström MC 2000. Is Northern China winning the battle against desertification? satellite remote sensing as a tool to study biomass trends on the Ordos Plateau in semiarid China. *Ambio* 29, 8, 468-476

Runnström MC 2003a. Rangeland development of the Mu Us sandy land in semiarid china: an analysis using landsat and NOAA remote sensing data. *Land Degradation & Development* 14, 2, 189–202

Runnström MC 2003b. Land degradation and migration in northern China evaluated from the biological production. Doctoral dissertation of Dept Physical Geography and Ecosystems Analysis, Lund University

Schlesinger WH 1991. Biochemistry: an analysis of global change. Academic Press, San Diego

Sellers P, Randall DA, Betts AH, Hall FG, Berry JA, Collatz GJ, Denning AS, Mooney HA, Nobre CA, Sato N, Field CB and Henderson-Sellers A 1997. Modelling the

exchanges of energy, water and carbon between continents and the atmosphere. *Science* 275, 502–509

Sellers P, Tucker CJ, Collatz GJ, Los SO, Justice CO, Dazlich DA and Randall DA 1994. A global 1 degree X 1 degree NDVI data set for climate studies. Part 2. *International Journal of Remote Sensing* 15, 17, 3519-3545

Sellers PJ 1985. Canopy reflectance, photosynthesis and transpiration. *International Journal of Remote Sensing* 6, 8, 1335-1372

Sellers PJ 1987. Canopy reflectance, photosynthesis and transpiration: II. The role of biophysics in the linearity of their interdependence. *Remote Sensing of Environment* 21, 143–183

Singh D, Herlin I, Berroir JP, Silva EF and Simoes Meirelles M 2004. An approach to correlate NDVI with soil colour for erosion process using NOAA/AVHRR data. *Advances in Space Research* 33, 3, 328-332

Singh D, Meirelles MSP, Costa GA, Herlin I, Berroir JP, Silva EF 2005. Environmental degradation analysis using NOAA/AVHRR data. *Advances in Space Research* (in press)

Stoms DM and Hargrove WW 2000. Potential NDVI as a baseline for monitoring ecosystem functioning. *International Journal of Remote Sensing* 21, 2, 401–407

Symeonakis E and Drake N 2004. Monitoring desertification and land degradation over sub-Saharan Africa. *International Journal of Remote Sensing* 25, 3, 573–592

Tanser FC and Palmer AR 1999. The application of a remotely-sensed diversity index to monitoring degradation patterns in a semi-arid, heterogeneous, South African landscape. *Journal of Arid Environments* 43, 4, 477-484

Tao B, Li KR, Shao XM, Cao MK 2003. The temporal and spatial patterns of terrestrial net primary productivity in China. *Journal of Geographical Sciences* 13, 2, 163-171

Thiam AK 2003. The causes and spatial pattern of land degradation risk in southern mauritania using multitemporal AVHRR-NDVI imagery and field data. *Land Degradation & Development* 14, 133–142

Tottrup C and Rasmussen MS 2004. Mapping long-term changes in savannah crop productivity in Senegal through trend analysis of time series of remote sensing data. *Agriculture, Ecosystems & Environment* 103, 3, 545-560

Tucker CJ and Newcomb WW, Los SO and Prince SD 1991a. Mean and inter-year variation of growing-season normalized difference vegetation index for the Sahel 1981-1989. *International Journal of Remote Sensing* 12, 6, 1133–1135

Tucker CJ 1980. Remote sensing of leaf water content in the near infrared. *Remote Sensing of Environment* 10, 23-32

Tucker CJ, Dregne HE and Newcomb WW 1991b. Expansion and contraction of the Sahara Desert from 1980-1990. *Science* 253, 299-301

Tucker CJ, Pinzon JE and Brown ME 2004. Global Inventory Modeling and Mapping Studies (GIMMS) satellite drift corrected and NOAA-16 incorporated Normalized Difference Vegetation Index (NDVI), monthly 1981-2002 The University of Maryland

UNCED 1992. Managing fragile ecosystems: Combating desertification and drought. Rep. No. Agenda 21, Chapter 12: United Nations Conference on Environment and Development

Wang J, Rich PM, Price KP and Kettle WD 2004. Relations between NDVI and tree productivity in the central Great Plains. *International Journal of Remote Sensing* 25, 16, 3127-3138

Watson RT 1999. Data management: databases and organization. Fourth edition, John Wiley & Sons, Inc.

Weiss E, Marsh SE and Pfirman ES 2001. Application of NOAA-AVHRR NDVI time-series data to assess changes in Saudi Arabia's rangelands. *International Journal of Remote Sensing* 22, 6, 1005-1027

Wessels KJ, Prince SD, Frost PE, van Zyl D 2004. Assessing the effects of human-induced land degradation in the former homelands of northern South Africa with a 1 km AVHRR NDVI time-series. *Remote Sensing of Environment* 91, 1, 47-67

WRB 2005. World reference base for soil resources, revised draft. ISRIC – World Soil Information, Wageningen

Wu JX 1996. Dongsheng coalfield's afforestation showing initial success. *Journal of Desertification Research* 16, 207–209

Wu W, Wang X, Yao F 1997. Applying remote sensing data for desertification monitoring in the Mu Us sandy land. *Journal of Desert Research* 17, 415–420 (in Chinese, abstract in English)

Zhang L, Wang FY, Zhang TJ 2002. Types and temporal-spatial change of desertized land in the Yulin area, northern Shaanxi. *Geology in China* 29, 4, 426-430

Zhu Z, Wang T 1993. Trends of desertification and its rehabilitation in China. *Desertification Control Bulletin* 22, 27–30

APPENDIX 1.   LAND DEGRADATION ASSESSMENT CRITERIA

Figure A below, used in the study by Liu *et al* (2003), covers part of Yulin Prefecture. It encompasses six counties: Dingbian, Jingbian, Hengshan, Yulin, Shenmu, Fugu with a total area of 17900 km^2 (see Fig.1a). This area was divided into 49 sub-areas (mainly depending on administrative towns/townships and referring to Chinas_ID in the data modelling).
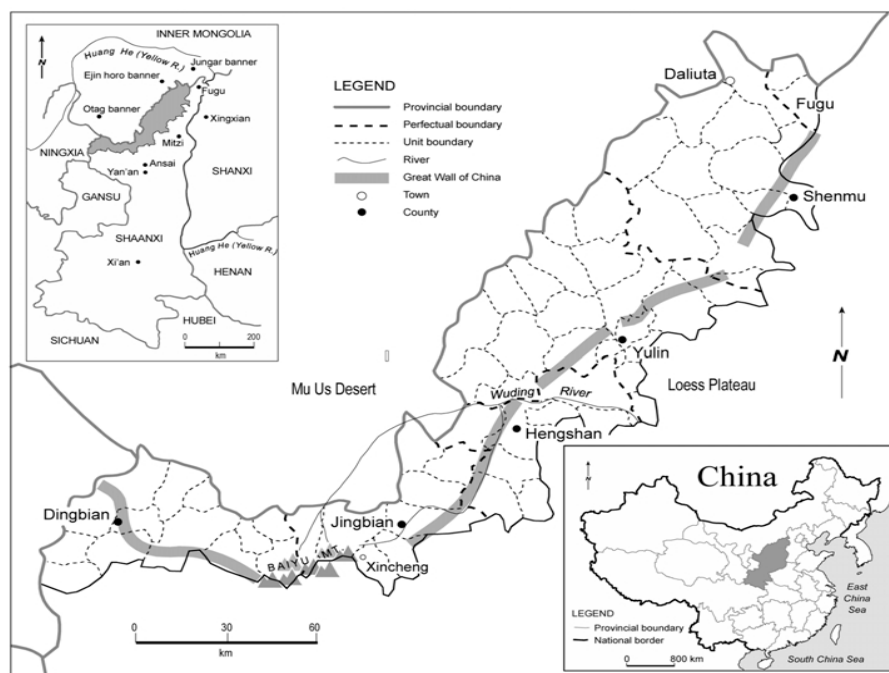

Fig. A: Study area used by Liu *et al.* (2003)

Table A: Indices and weights for factors used in the assessment of land degradation

Indicators	Severity level				Weight
(%)	I–severe	II–high	III–medium	IV–low	
Vegetation cover	<10	10–25	25–40	>40	0.40
Drifting sand coverage	>65	15–65	5–15	<5	0.25
Annual desertification rate	>5	2–5	1–2	<1	0.15
Population pressure	>50	30–50	0–30	−30–0	0.20

Table B: Area of degraded land within the study area (10^4 ha)

Area studied		Severity level							
		I – severe		II – high		III – medium		IV – low	
Total area	%	Area	%	Area	%	Area	%	Area	%
179.36	100	111.03	61.90	39.96	22.28	6.42	3.58	21.95	12.24
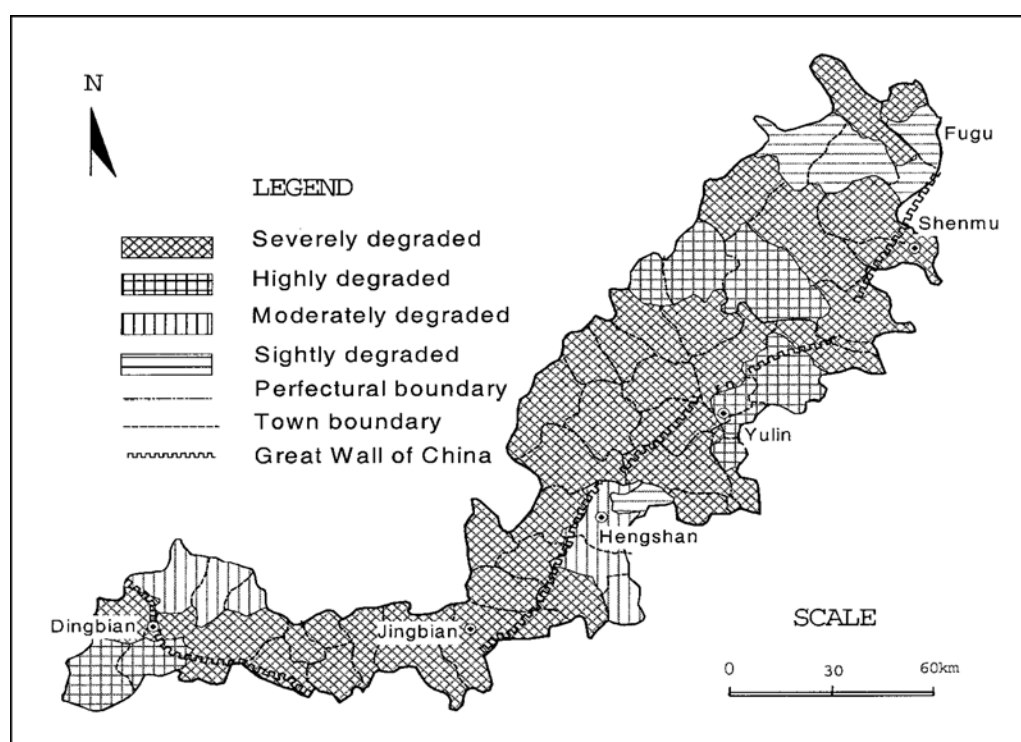
Fig. B: Spatial distribution of land degradation status (after Liu *et al.* 2003)

APPENDIX 2.   ABBREVIATIONS

AF	ArisFlow
CEVSA	Carbon Exchange between Vegetation, Soil, and the Atmosphere
CoV	Coefficient of Variation
FPAR	Fraction of Photo-synthetically Active Radiation absorbed by the green canopy
GIMMS	The Global Inventory Modelling and Mapping Studies
GLADA	Global assessment of Land Degradation and improvement
GLASOD	Global Assessment of human-induced Soil Degradation
HANTS	Harmonic Analyses of NDVI Time-Series
ISLSCP	International Satellite Land Surface Climatology Project
LAIg	Green Leaf Area Index
MS Access	Microsoft Access
NDVI	Normalized Difference Vegetation Index
NOAA AVHRR	National Oceanic and Atmospheric Administration Advanced Very High Resolution Radiometer
NPP	Net Primary Productivity
NPV	Non-Photosynthetic Vegetation
PV	Photosynthetic Vegetation
RUE	Rain-Use efficiency
RVC	Rate of Vegetation Coverage
RVI	Ratio Vegetation Index
SiB	Simple Biosphere model
SQL	Structured Query Language
UNCCD	United Nations Convention to Combat Desertification